

Aus dem Institut für Experimentelle Ophthalmologie
der Medizinischen Fakultät
der Universität des Saarlandes, Homburg/Saar
Direktor: Prof. Dr. hum. biol. Achim Langenbucher

Prüfung der mechanischen Schutzwirkung,
Oberflächenqualität und Refraktion von
Arbeitsschutzbrillen

Dissertation zur Erlangung des Grades eines Doktors
der Naturwissenschaften
der Medizinischen Fakultät
der Universität des Saarlandes
2013

vorgelegt von

Alexis Michael Speck
geb. am: 13.10.1986 in Blasendorf

Für Eduard, Julica und Georg

Inhaltsverzeichnis

1	Zusammenfassung	1
2	Einleitung und Motivation	3
3	Veröffentlichung 1: Experimental assessment of eye protection efficiency against high speed projectiles	10
4	Veröffentlichung 2: Inspection of freeform intraocular lens topography by phase measuring deflectometric methods	17
5	Veröffentlichung 3: Theoretical model for design and analysis of protective eyewear	26
6	Literaturverzeichnis	36
7	Publikationsverzeichnis	39
8	Danksagung	42

1 Zusammenfassung

Arbeiten oder Tätigkeiten mit potentiellen thermischen, chemischen oder mechanischen Gefahren müssen mit einem adäquaten Augenschutz durchgeführt werden. Sogenannte Arbeitsschutzbrillen werden in der Regel im Spritzgussverfahren hergestellt. Der optischen Abbildungsqualität wird jedoch bei der Herstellung nicht in ausreichendem Umfang Rechnung getragen, so dass eine bessere Sicht dem Augenschutz Vorrang gewährt. Die Folge ist eine mangelnde Trageakzeptanz.

Im Rahmen der Optimierung solcher Arbeitsschutzbrillen wurden differenzierte Prüfmethoden entwickelt. In der vorliegenden Arbeit werden 3 Bereiche vorgestellt: Ein System zur mechanischen Endkontrolle von Schutzbrillen gegen Hochgeschwindigkeitsprojektil, ein Geometriemessplatz zur berührungslosen Vermessung der Spritzgussformen und Polycarbonatscheiben, sowie eine Optimierungsplattform zur Prüfung und Verbesserung der optischen Qualität von Schutzbrillen.

Um frei ausrichtbare und beliebige Objekte mit hohen Geschwindigkeiten auf einen Testkopf samt Schutzbrille beschleunigen zu können, wurde ein frei bestückbares Beschusssystem aufgebaut. Das System erreichte Geschwindigkeiten bis zu 62 m/s bei einer maximalen Projektilgröße von $30\text{ mm} \times 30\text{ mm} \times 40\text{ mm}$.

Zur Vermessung der Spritzgusswerkzeuge und Polycarbonatscheiben wurde ein kommerzielles berührungsloses Messsystem weiterentwickelt und für duosphärische und Vollformscheiben bis 180 mm Durchmesser validiert. Genauigkeit und Auflösungsgrenzen wurden für reflektierende Kunststoffoberflächen mit Radien außerhalb der Spezifikation ermittelt. Mit dem System wurden kommerzielle Schutzbrillen vermessen und deren Modelldaten extrahiert. Die optische Qualität der Scheiben wurde mit der Optimierungsplattform überprüft. Durch einen Optimierungsalgorithmus konnte der Wellenfrontfehler von kommerziellen Schutzbrillen nochmals verringert werden.

Mit den durchgeführten und entwickelten Untersuchungsmethoden kann eine Qualitätsverbesserung der Schutzbrillen erreicht werden. Die Trageakzeptanz kann dadurch möglicherweise erhöht werden.

Summary - protection efficiency, surface quality and refraction testing of occupational eyewear

The protection with safety goggles is required for work with possible chemical, thermal or mechanical hazards. Occupational eye wear such as safety goggles are usually manufactured by injection molding techniques. The production process mainly focuses on safety aspects, despite the high importance of the optical quality. The major consequence is a lack of wearer acceptance.

A sophisticated process chain was built within the framework of optimizing the safety goggles. In the presented work, three parts of the process chain are being introduced: A system for testing the eye protection efficiency of safety goggles against high speed projectiles, a surface inspection for measuring injection molds and their spectacles and a simulation platform for optimizing the optical quality of safety goggles.

The catapult system for the final verification was used to load projectiles of up to $30\text{ mm} \times 30\text{ mm} \times 40\text{ mm}$ in size with arbitrary orientation for shooting at a test head, which is wearing safety goggles. Velocities up to 62 m/s could be realized.

A commercial measurement system was adapted to our requirements and optimized for measuring injection molding tools and polycarbonate spectacles. The evaluation was performed for duospherical and full form spectacle lenses with an lateral field of 180 mm . Threshold and resolution were determined for specular reflective plastic surfaces with radii beyond the specifications. Commercial safety goggles were measured and model design data could be derived with the system. The optical quality of the model was cross checked with a simulation platform and the wavefront error of the commercial goggles could be improved.

With the investigations and the developed methods a quality optimization of safety goggles could be reached and the wearer acceptance may be improved significantly.

2 Einleitung und Motivation

Das Sehen schützen - schon seit jeher üben Menschen Tätigkeiten aus, bei denen das Auge potentiellen Gefahren ausgesetzt ist. Die erste Schutzbrille wurde im 17. Jahrhundert zum Schutz vor starkem Sonnenlicht entwickelt. Der Begriff Arbeitsschutz tauchte im 19. Jahrhundert in Preußen auf und die Arbeitsschutzbrille, so wie wir sie kennen, wurde erst Jahre später ab 1930 produziert [15]. Heutige Arbeitsschutzbrillen sollen vor chemischen, mechanischen oder thermischen Einflüssen schützen. Trotz der Tragepflicht, vor allem in Betrieben vorgeschrieben durch Unfallverhütungsvorschriften (UVV), geltende Verordnungen (BGV A1) und berufsgenossenschaftliche Regeln für Sicherheit und Gesundheit bei der Arbeit (BGR), ermittelt der Hauptverband der gewerblichen Berufsgenossenschaften etwa 36.000 meldepflichtige Augenverletzungen pro Jahr [2, 16]. Insgesamt belaufen sich Augenverletzungen auf rund 300.000 Fälle jährlich. Gerade der Sehverlust hat eine hohe volkswirtschaftliche Bedeutung, bemessen an einem Grad der Behinderung von 40% durch Verlust eines Auges [4]. Typische Unfallszenarien ergeben sich durch Handmaschinen/-werkzeuge wie z.B. Schneidemaschinen für Nahrungs- und Genussmittel, Kreissägen aller Art, Pressen und Stanzen sowie bekannte Metallbearbeitungswerkzeuge (Drehmaschine, Bohrmaschine, Fräsmaschine, usw.) [18]. Nahezu 50% der Unfälle mit Handwerkzeugen entstehen durch klassische Klingen und Messer, Hammer, Meisel und Schraubenschlüssel/-dreher. Zu den typischen Verletzungsmustern gehören Kontusionsverletzungen wie z.B. (stumpfe) Bulbustraumata, bis hin zu Perforationen oder Bulbusberstungen mit Cornea-/Skleraperforation sowie Iris-, Glaskörper und Retinaprolaps. Im Extremfall führen diese zur Enukleation des Augapfels. Gerade scharfkantig abgebrochene oder spitze Teile und Partikel, entstanden durch Kreissägen, Stanzen und Pressen, führen häufig zu schwerwiegenden penetrierenden und perforierenden Verletzungsmuster. Dabei sind 90% der Fälle vermeidbar und können durch Tragen des richtigen Augenschutzes verhindert werden [3, 9, 11, 12].

Hierbei stellt sich oft die Frage: Weshalb wurde die Schutzbrille nicht getragen?

Schutzbrillentypen, -klassen und normative Aspekte

Bei der Auswahl der richtigen Schutzbrille muss der Einsatzzweck bekannt sein. Daraus ergibt sich die Frage ob die Schutzbrille der äußeren (chemischen, thermischen oder mechanischen) Wirkung standhalten würde. Dieser Abschnitt behandelt Schutzbrillentypen und deren Klassen im normativen Umfeld, beschränkt auf mechanische äußere Einwirkung und die optische Qualität. An dieser Stelle soll erwähnt werden, dass thermische und chemische Einflüsse normativ sehr gut erfasst werden. Grundlegend gibt es aber kaum Übereinstimmung zwischen normativen Tests und realen Unfallszenarien für eine mechanische Einwirkung. Schutzbrillenhersteller halten sich daher auch sehr bedeckt bzgl. definierter Einsatzzwecke für die verschiedenen Brillenmodelle. Hier wird auf Regularien (BGR 192), Verordnungen (BGV A1) und Unfallverhützungsvorschriften (UVV) verwiesen, die ebenfalls keinerlei Hinweise zu den genauen Einsatzzwecken geben. In der DIN-Norm für persönlichen Augenschutz werden mechanische Einflüsse als Stöße verschiedener Energie berücksichtigt. Dabei gibt es 3 Arten von Augenschutzgeräten: Bügelbrillen mit oder ohne Seitenschutz, Korbbrillen und Gesichtsschutzschilde (DIN EN 166) [6]. Abbildung 1 zeigt Schutzbrillenmodelle (Bügelbrille) für Projektgeschwindigkeiten bis $45 \text{ m} \cdot \text{s}^{-1}$ (links) und als Korbbrille bis $120 \text{ m} \cdot \text{s}^{-1}$ (rechts).



(a) Ausführung einer Bügelbrille mit duosphärischer Polycarbonatscheibe bis $45 \text{ m} \cdot \text{s}^{-1}$.

(b) Monosphäre als Korbbrille für den Vollschutz bis $120 \text{ m} \cdot \text{s}^{-1}$.

Abbildung 1: Zwei Brillenmodelle für den Augenschutz gegen mechanische, thermische oder chemische Einflüsse (je nach Beschichtung und Materialzusammensetzung).

In DIN-, ANSI- und ISO-Normen werden Mindestfestigkeiten, erhöhte Festigkeiten, oder Beständigkeit gegen kleine und große Teilchen mit niedriger und hoher Geschwindigkeit unter verschiedensten Einschlag- und Aufprallszenarien definiert. Allerdings werden hierfür immer definierte Stahlkugeln oder Projektiler als Prüfkörper mit bestimmten Geschwindigkeiten oder Energien verwendet [1, 6, 7]. Pe-

netrierende und stumpfe Traumata mit willkürlich geformten oder scharfkantigen Teilchen bei extrem hohen Geschwindigkeiten werden z.B. nicht von der Norm erfasst [14, 17, 26]. Ein wesentlicher Punkt in den Normen bezieht sich auf die optische Qualität und optische Prüfverfahren für Schutzbrillengläser. Differenziert wird zwischen einer Vielzahl an optischen Prüfverfahren, deren Ergebnisse den Anforderungen gerecht werden müssen. Grundsätzlich sind für die optische Klasse 1 eine sphärische und astigmatische Wirkung unter $0,06\text{ D}$ zulässig, bei ophthalmischen Gläsern (z.B. refraktionskorrigierende Sehhilfen) sind dagegen Werte bis $0,12\text{ D}$ zulässig. Ebenfalls wird die prismatische Wirkung, die prismatische Wirkungsdifferenz und der Lichttransmissionsgrad berücksichtigt. Durch die verwendeten Testsysteme können jedoch nur Aberrationen niederer Ordnung und die subjektive optische Qualität anhand von "pass/fail"-Kriterien bestimmt werden [1, 6–8, 19, 20]. Gerade die durch die Herstellung entstehenden Aberrationen höherer Ordnung führen zu einer schlechteren optischen Abbildungsqualität, die kaum erfasst und nicht quantifiziert werden kann. Dies kann wiederum zu somatischen Wirkungen wie Schwindel, Kopfschmerz oder Übelkeit führen. Die Folge ist eine mangelnde Trageakzeptanz, selbst bei Premiumprodukten der optischen Klasse 1 [12, 25]. Gründe hierfür sind vor allem im Spritzgussprozess, in der Beschichtung und in der Assemblierung der Scheiben, zu suchen.

Herstellung von Arbeitsschutzbrillen

Arbeitsschutzbrillen werden im Spritzgussverfahren hergestellt. Abbildung 2 zeigt den allgemeinen Stand der Technik für die Prozesskette. Das Optikdesign bildet die Basis für die Herstellung von sogenannten Spiegeleinsätzen für das Spritzgusswerkzeug, konform nach industriellen Standards und deren Anforderungen (DIN EN 166 Persönlicher Augenschutz) [1, 6, 19, 32]. Mit einem Satz dieser Spiegeleinsätze können 50.000 bis zu 250.000 Scheiben produziert werden, bis eine Überarbeitung notwendig ist. Nach dem Spritzgussprozess werden die Scheiben je nach Anwendung und Einsatzzweck beschichtet und mit einer Fassung versehen (assembliert). Die Qualität der Endprodukte wird nach DIN EN 167 / ISO 4849 oder ANSI Z87 geprüft [8, 24]. Wie im vorangegangenen Abschnitt erwähnt, handelt es sich dabei um eine teils subjektive Klassifizierung die nur eine beschränkte Aussage über die Qualität der Scheibe zulässt [10]. Die Evaluation der Oberflächenqualität der Spiegeleinsätze wird empirisch während der Prozessparametrierung durchgeführt. Während dieses iterativen Prozesses wird eine hohe Quantität an Scheiben produ-

ziert, die mechanisch und optisch geprüft werden muss. Wenn die Normkonformität nicht erreicht wird, werden die Spiegeleinsätze erneut überarbeitet. Die tatsächliche Oberfläche der Spiegeleinsätze kann mangels fehlender Prozessüberwachung nicht geprüft werden.

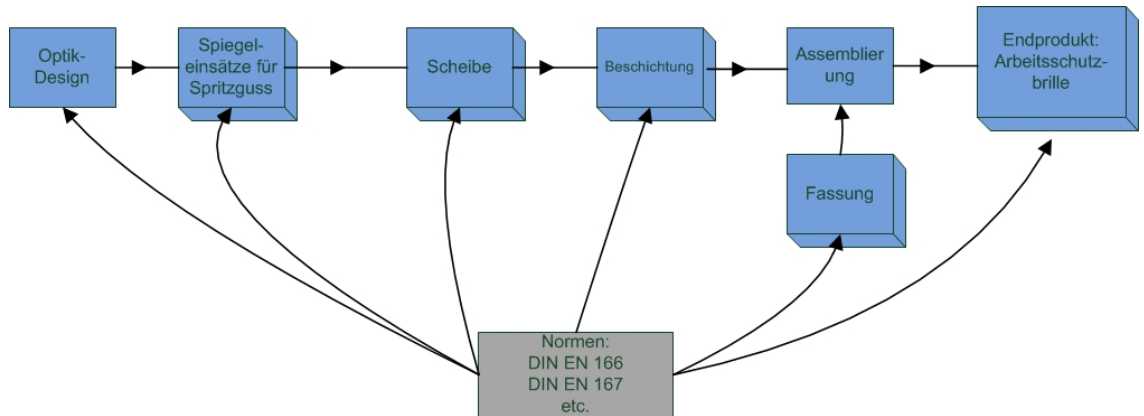


Abbildung 2: Prozesskette für die Herstellung von Arbeitsschutzbrillen.

Im Rahmen meiner Arbeit zum Thema Optimierung von Arbeitsschutzbrillen wurden folgende Untersuchungen durchgeführt und in peer-review Journalsen publiziert (Vollständige Auflistung siehe Publikationsverzeichnis):

1. Oberflächenprüfung

- Deflektometrie zur Analyse von Spritzgusswerkzeugen für die Schutzbrillenherstellung / *Deflectometric analysis of high volume injection molds for production of occupational eye wear*
- Deflektometrie zur Oberflächeninspektion und Formtreueuntersuchung für die Herstellung und Politur von Arbeitsschutzbrillen / *Deflectometry for surface inspection and shape fidelity analysis for manufacturing and polishing of safety spectacle molds*
- Deflektometrie zur Topographiemessung von Kunststoffoptiken am Beispiel der Intraokularlinse / *Inspection of freeform intraocular lens topography by phase measuring deflectometric methods*
- Deflektometrie zur Qualitätskontrolle der Polycarbonatscheiben von Arbeitsschutzbrillen / *Quality control of injection molded eyewear using non-contact deflectometry*

2. Simulation

Theoretisches Modell für die Optimierung und Analyse von Schutzbrillen /
Theoretical model for design and analysis of protectional eyewear

3. Wellenfrontprüfung

Wellenfrontanalyse von Arbeitsschutzbrillen / *Wave-front analysis of personal eye protection*

4. Photochromieprüfung

Photochromieprüfung von ophthalmischen Linsen / *Photochromic dynamics of ophthalmic lenses*

5. Endkontrolle zur Schlagfestigkeit

System zur Prüfung von Schutzbrillen gegen Hochgeschwindigkeitsprojektile / *Experimental assessment of eye protection efficiency against high speed projectiles*

Dabei wurde eine differenzierte Prozesskette für die Herstellung von Arbeitsschutzbrillen entwickelt (siehe Abbildung 3). In der vorliegenden Dissertationsschrift finden 3 der Untersuchungen Eingang (schraffiert dargestellt).

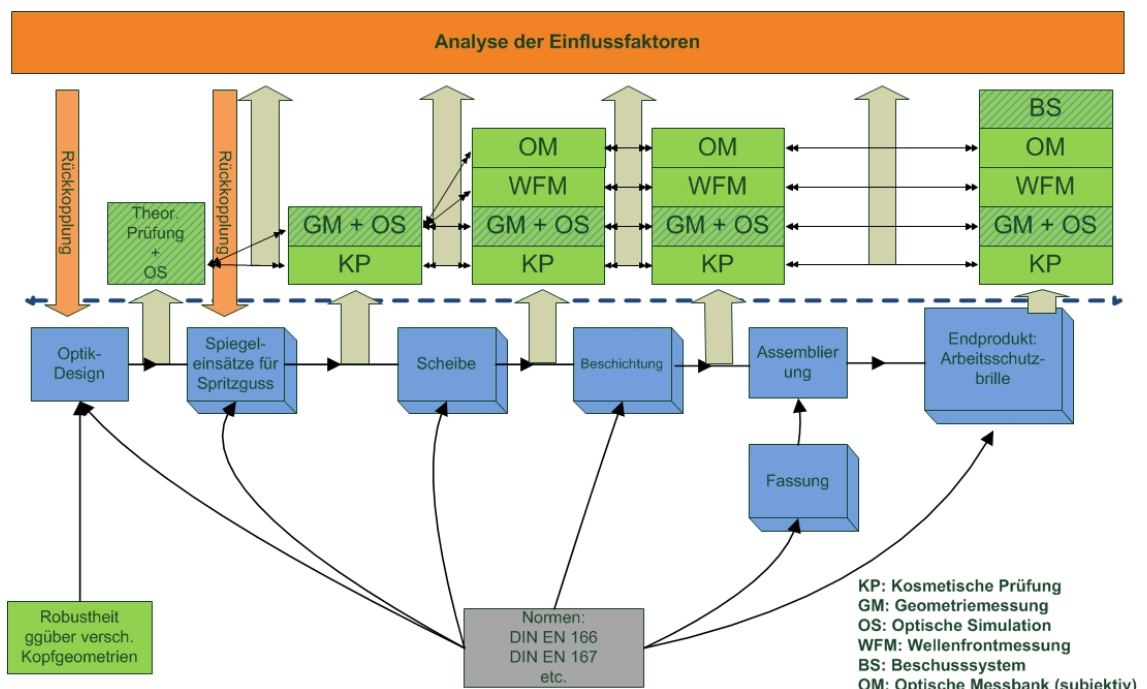


Abbildung 3: Differenzierte Prozesskette für die Herstellung von Arbeitsschutzbrillen. Die Bestandteile dieser Dissertation sind schraffiert gezeigt (Geometriemessung, optische Simulation und Beschusssystem)

System zur Prüfung von Schutzbrillen gegen Hochgeschwindigkeitsprojektile (Veröffentlichung 1)

In der ersten Veröffentlichung wird ein System zur Untersuchung der Schutzwirkung von Sicherheitsbrillen gegen Hochgeschwindigkeitsprojektile beschrieben. Gemäß geltender deutscher Normen müssen Schutzbrillen mechanischen Einwirkungen gewissen Grenzen standhalten. Klassifiziert wird zwischen einer Mindestfestigkeit, einer erhöhten Festigkeit mit frontalem und seitlichem Aufprall und einer Prüfung zum Schutz gegen Teilchen mit hoher Geschwindigkeit. Bügelbrillen dürfen hier maximal mit einem Stoß mit niedriger Energie von $45 \text{ m} \cdot \text{s}^{-1}$ ($0,86 \text{ g}$ Stahlkugel mit dem Nenndurchmesser von 6 mm) belastet werden. Generell werden für alle Prüfverfahren Kugeln verwendet. Keine der ANSI, DIN oder ISO Prüfverfahren decken beliebige, schwere und mit hoher Geschwindigkeit auf die Polycarbonatscheibe auftreffende Objekte ab [1,6,7,19]. Die Fachliteratur spricht ebenfalls nur von speziellen Projektilen, Kugeln oder Schrot mit definierten Orientierungen und Aufschlagmomenten [5,27,28]. Um frei ausrichtbare und beliebige Objekte mit hohen Geschwindigkeiten auf einen Testkopf samt Schutzbrille beschleunigen zu können, wurde im Rahmen dieser Arbeit ein frei bestückbares Beschussystem aufgebaut. Das System besteht aus einem Seilzugsystem mit fünf Umlenkpunkten. Ein Schlitten (Objektträger) wird auf einer 3 m langen Rampe beschleunigt und die Geschwindigkeit wird zum Zeitpunkt der Auslösung des Projektils vom Schlitten mit einer Mikrolightschranke gemessen. Das Ergebnis wird über ein digitales Speicheroszilloskop, eine Slow-Motion Kamera und eine Hochgeschwindigkeitskamera dokumentiert. Es werden Geschwindigkeiten von bis zu $62 \text{ m} \cdot \text{s}^{-1}$ bei einer maximalen Projektilgröße von $30 \text{ mm} \times 30 \text{ mm} \times 40 \text{ mm}$ erreicht.

Vermessung und Optimierung von Schutzbrillenscheiben (Veröffentlichung 2 & 3)

Die zweite und dritte Veröffentlichung behandeln die Oberflächenprüfung und die Optimierung eines Schutzbrillenmodells. Zur Vermessung der Schutzbrillenoberflächen wurde ein kommerzielles Messsystem weiterentwickelt, basierend auf der phasenmessenden Stereo-Deflektometrie (PMD). Für die absolute Positionsmeßung im Raum sind zwei Kameras auf ein effektives Messfeld von $80 \times 80 \text{ mm}^2$ eingestellt ($f' = 16 \text{ mm}$, Standard PMD-Sensor) [13,21–23]. Der Standard PMD-Sensor wurde

bisher nur für die Ermittlung von Krümmungsdaten von Glaslinsen verwendet. An dieser Stelle sollten thematisch drei weitere Publikationen zur Oberflächenprüfung von Spritzgusswerkzeugen und Polycarbonatscheiben erwähnt werden (a, b, d). Das Oberflächenmesssystem wurde in einer Arbeit für einfache und übergroße Spiegeleinsätze validiert (b). Je nachdem ob es sich um ein duosphärisches Modell oder eine Vollformscheibe handelt, werden Messfelder von bis zu 180 mm in lateraler Richtung benötigt. Dafür wurde eine zusätzliche Kamera mit einer Objektivbrennweite von $8,5\text{ mm}$ in den Messaufbau integriert und die phasenmessende Deflektometrie auf insgesamt drei Kameras erweitert [30]. In zwei weiteren Arbeiten (a, d) wurden die Auflösungsgrenze und die Genauigkeit der unterschiedlichen Kameras für Spiegeleinsätze und für Polycarbonatscheiben unter Einsatz eines fünfachsig referenzierten Positioniersystems ermittelt [29, 31]. In der vorliegenden Dissertationsschrift wird die Validierung für reflektierende Kunststoffoberflächen und Radien außerhalb der genannten Spezifikation ($\text{Radien} < 40\text{ mm}$) anhand von Intraokularlinsen (IOLs) gezeigt. In der dritten hier vorgestellten Veröffentlichung wurden anschließend drei kommerziell verfügbare Schutzbrillen vermessen. Damit können vier Topographien (Vorder- und Rückseite für jeweils beide Augen) aufgenommen werden, sowie Modelldaten extrahiert werden. Die optische Qualität der generierten Modelldaten wurde anschließend in einem Optiksimulationsprogramm (Raytracer) anhand normkonformer optischer Kenngrößen geprüft (sphärische Wirkung, astigmatische Wirkung, prismatische Wirkungsdifferenz). Eine Besonderheit war die über die Normprüfung hinausgehende Berücksichtigung des Wellenfrontfehlers in fünf Blickrichtungen. Mit einer Optimierung der Designdaten konnte der Wellenfrontfehler der drei kommerziellen Schutzbrillenmodelle nochmals verringert werden. Der Algorithmus basiert auf einer iterativen Anpassung der Rückfläche samt Rückflächenlage bei Beibehaltung der Vorderfläche und der Dicke der Scheibe unter Beachtung normkonformer optischer Kenngrößen sowie des Wellenfrontfehlers.

3 Veröffentlichung 1

TECHNISCHE MITTEILUNG

Experimental assessment of eye protection efficiency against high speed projectiles

Alexis Speck*, Benedikt Zelzer, Timo Eppig, Achim Langenbucher

Experimental Ophthalmology, Saarland University, Kirrberger Straße 100, 66424 Homburg/Saar, Germany

Received 4 April 2012; accepted 18 June 2012

Abstract

Introduction: Work in hazardous zones with the risk of mechanical injuries requires protection with safety spectacles. Mechanical eye injuries with metal foreign bodies are often caused by rotational material machining or production processes with high pressure or high velocity moving parts. Normative regulations restrict to tests with small and fast flying objects (e.g. 6 mm ball). The literature does not provide any information about protection capabilities against larger objects with high mass and arbitrary shape. The purpose of this study was to test the protection efficiency of safety spectacles against flying objects. The scope of this paper is to present a new test setup for mechanical impact resistance testing of personal protective eyewear against objects with arbitrary shape and mass.

Material and Methods: The setup is based on a catapult platform, accelerating a sliding carriage on a rail. A pull rope system allows velocities up to $62 \pm 2 \text{ m}\cdot\text{s}^{-1}$. A photo sensor was used for velocity measurement. The carriage can be loaded with projectiles of up to $30 \text{ mm} \times 30 \text{ mm} \times 40 \text{ mm}$ in size with arbitrary orientation, depending on the carriage insert. Testing and validation was done with projectiles such as 7 g metal chips and fragments with approximate dimensions of $10 \text{ mm} \times 15 \text{ mm}$. Samples were standard occupational safety spectacles mounted on a test head. The projectile impact was captured with a monochrome high speed camera.

Experimentelle Untersuchung zur Schutzwirkung von Sicherheitsbrillen gegen Hochgeschwindigkeitsprojekteile

Zusammenfassung

Einleitung: Arbeiten oder Tätigkeiten im potentiellen Gefahrenbereich, in dem die Möglichkeit einer mechanischen Gefährdung vorliegt, müssen mit einem adäquaten Augenschutz durchgeführt werden. Materialbearbeitung oder allgemein Produktions- und Fertigungsprozesse sind eine häufige Ursache für Augenverletzungen durch metallische Fremdkörper. Normative Anforderungen begrenzen sich auf Versuche mit kleinen definierten Objekten, wie zum Beispiel 6-mm-Stahlkugeln für einen Aufpralltest. Informationen über die Widerstandsfähigkeit gegen beliebig große und schwere Objekte und Projekteile sind in der Literatur nicht zu finden.

Diese Arbeit beschreibt einen neuen Versuchsaufbau, mit dem die mechanische Schutzwirkung von Sicherheitsbrillen gegen Fremdkörper mit beliebiger Form und Masse geprüft werden kann.

Material und Methoden: Der Versuchsaufbau basiert auf einer Beschussrampe, bestehend aus einem Beschleunigungsschlitten samt Führungsschiene und einem Seilzugsystem. Damit sind Geschwindigkeiten bis zu $62 \pm 2 \text{ m}\cdot\text{s}^{-1}$ möglich, gemessen durch eine Lichtschranke am Ende des Beschleunigungsweges. Der Schlitten nimmt

* Corresponding author: Alexis Speck, Experimental Ophthalmology, Saarland University, Kirrberger Straße 100, 66424 Homburg/Saar, Germany.
E-mail: alexis.speck@mx.uni-saarland.de (A. Speck).

Results: The aiming accuracy test showed deviations of approximately 1 mm of two impacts on the same spectacle surface with a free flight distance of 150 mm. All tests with slow, medium and high speed projectiles showed no contact with the eye medium. Objects with velocities from 10 m·s⁻¹ to 62 m·s⁻¹ fired the spectacle off from the test head. The medium speed test cut off one side of the spectacle frame. The high speed test with 62 ± 2 m·s⁻¹ cracked the polycarbonate shield.

Discussion: We describe a method for accelerating arbitrary objects up to 62 m·s⁻¹ and for aiming these objects on safety eyewear, mounted on a test head. The setup allows a variety of projectile shapes, orientations and velocities. The accuracy of velocity measurement is ± 2 m·s⁻¹ for high velocity (< ± 5%). Further studies will address optimization of this setup due to signs of wear and gliding properties of the carriage, wireless ignition and higher velocities.

Keywords: Safety goggles, eye protection, mechanical hazard, experimental test setup

Projektile mit maximal 30 mm × 30 mm × 40 mm und beliebiger Beschusslage auf. Für die Validierung und die Messreihen wurden 7 g schwere Metallprojektile und Fragmente mit einer ungefähren Größe von 10 mm × 15 mm verwendet. Beschossen wurden Standardschutzbrillen, montiert auf einem Testkopf. Der Objekteinschlag wurde durch eine monochrome Hochgeschwindigkeitskamera dokumentiert.

Ergebnisse: Die Zielgenauigkeit liegt bei ungefähr 1 mm Abweichung, bezogen auf zwei aufeinanderfolgende Einschläge mit einer 150-mm-Freiflugphase. Keiner der Versuche führte zum Durchschlag und damit zum Augenkontakt mit dem Projektil. Bei allen Tests mit Geschwindigkeiten von 10 m·s⁻¹ bis 62 m·s⁻¹ wurde die Schutzbrille vom Testkopf geschleudert. Ein Versuch mit mittlerer Geschwindigkeit trennte eine Seite des Brillenrahmens ab. Der Hochgeschwindigkeitsversuch mit 62 ± 2 m·s⁻¹ führte zu einem Riss in der Polycarbonatscheibe.

Diskussion: In dieser Arbeit beschreiben wir eine Methode zur definierten Beschleunigung und zum Beschuss von Schutzbrillen mit beliebigen Objekten. Der Versuchsaufbau ermöglicht eine Vielzahl von Projektilformen, -lagen und -geschwindigkeiten. Die Messgenauigkeit beträgt ± 2 m·s⁻¹ für hohe Geschwindigkeiten (< ± 5%). Folgende Studien beschäftigen sich mit der Optimierung des Aufbaus im Hinblick auf Verschleißerscheinungen und Gleiteigenschaften des Schlittens, einer kabellosen Fernzündung und mit höheren Geschwindigkeiten.

Schlüsselwörter: Schutzbrillen, Augenschutz, mechanische Gefährdung, experimenteller Versuchsaufbau

Introduction

Working conditions, such as in mechanical workshops or in laboratories, require adequate eyewear protecting against mechanical hazards [1]. Mechanical eye injuries with metal objects are often caused by rotational material machining, e.g. drilling, turning, milling, grinding, sawing or production processes with high pressure or high velocity like punching, compacting or cutting. Typical blunt and penetrating eye injuries in industrial processes with metallic objects affect the cornea, sclera, lens and iris [2,3].

We performed a technical review in terms of testing the protection efficiency of eye safety goggles against large and heavy fast flying objects, which are not covered in the respective ANSI / DIN / ISO normative regulations. The requirements concerning the protective effect of personal eye protection mainly refer to DIN EN 166 and ANSI Z 87.1 [4,5]. For spectacles there is a minimum resistance test with a 22 mm steel bullet with a force of 100 ± 2 N, a higher resistance test with

a bullet mass of 43 g at a speed of 5.1 m·s⁻¹ and requirements for high – speed bullets with a mass of 0.86 g accelerating up to 45 + 1.5 m·s⁻¹ [6]. ANSI Z 87.1 also describes standardized test methods like mass impact, drop – ball impact and velocity impact tests with missiles and steel balls with velocities from 45.7 to 91.4 m·s⁻¹. The norm differentiates between speed, size, mass and impact location of the bullets, depending on the spectacle, shield and goggle type.

ANSI / DIN / ISO regulations restrict to tests with small high - weight high - speed particles and the literature does not provide any information about protection capabilities against larger and high mass objects. In the literature, impact tests are used only for defined shapes, e.g. simulation of glass particles or for devices with DIN / ISO conformity to standardized bullets, missiles or balls. Typical tests are based on a ballistic apparatus, e.g. (pump) air guns or nitrogen guns [7–11].

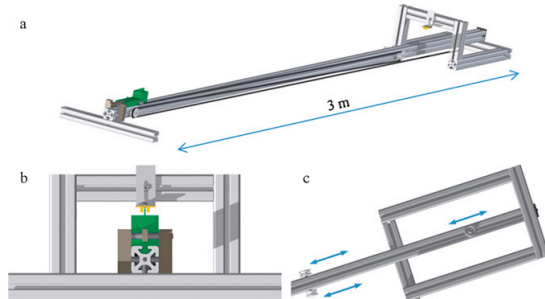


Figure 1. a) Overview of the launching platform with hooked carriage and expanded Bowden cable on the right side, used for acceleration foreign bodies up to $62 \text{ m}\cdot\text{s}^{-1}$. b) Detail view of the carriage plate and the photo interrupter, for measuring the velocity of the carriage projectile. c) Adjustable ball bearing roller on the bottom side, changing cable settings and speed (blue arrow).

In this technical note we describe the construction, implementation and validation of a new test setup for mechanical impact resistance testing of personal protective eyewear in terms of high speed foreign bodies with arbitrary shape and mass.

Material and Methods

Launching platform

The setup is based on a launching platform with a pull rope system, accelerating a sliding carriage on a rail. It is separated in a 2.3 m acceleration and 0.7 m deceleration distance with an additional bumper at the end. The base construction was built from a $40 \times 40 \text{ mm}$ standard aluminum rail, as seen on Figure 1. Figure 1c shows the bottom side with one of five

ball bearing rollers, which are all fixed with moveable sliding blocks for varying acceleration and decelerating tracks. The rollers were used to guide the Bowden cable and to reach a higher drag force by expanding the cable acceleration and deceleration range over the whole distance of the rail (about 6 times). Four of them were side mounted and the last roller was mounted on the bottom to turn around the Bowden cable. The maximum cable span length for the acceleration is about 15 m, using all rollers in the furthest position. Working tensions were from 200% up to 600%, according to the material properties. For the Bowden cable we used different materials, e.g. gummed counter rope (sailing rope), hollow rubber or tube and pipe caoutchouc rubber (EMC-Megarubber Scale-Bungee from model building), depending on the velocity.

The carriage

Figure 2a and b show the low - weight carriage with the guide rail on the bottom. The material is Polyoxymethylene (POM), due to the weight and the gliding properties (low friction) on the aluminum base. Figure 1b shows the carriage fixation in the slide. The mass of the carriage including metal parts was 128 g. The carriage can load projectiles up to $30 \text{ mm} \times 30 \text{ mm} \times 40 \text{ mm}$ in size, with an optional foam inlay, depending on the projectile shape and orientation.

Velocity measurement

For velocity measurement, the carriage is designed with a black plate on the top. With a light barrier and the defined length of the plate, we could calculate the actual velocity of the carriage when changing from acceleration to deceleration (maximum speed). For the edge detection we used a photo interrupter (Sharp OPIC Photointerrupter GP1A53HR, 5 mm standard gap), additional enhanced gap and a digital memory

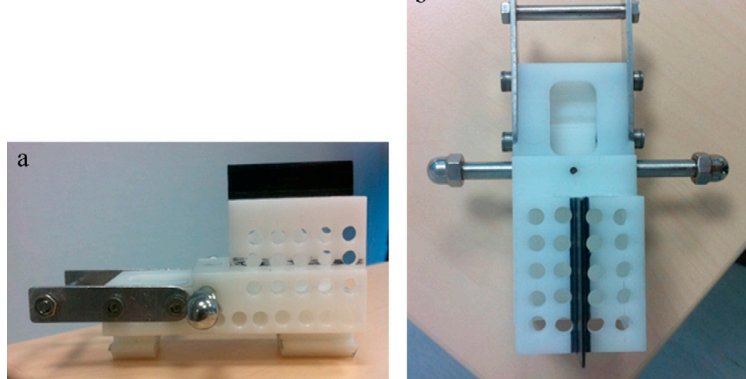


Figure 2. Side view and top view of the low - weight carriage with the detector plate, hinge bar, Bowden cable fixation and guide rail on the bottom.

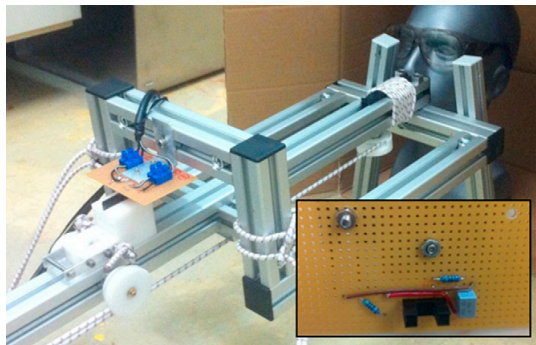


Figure 3. Launching platform with installed velocity detector, including enhanced photo interrupter and electronic parts on the mounting plate (backside). For test procedure a gummed counter rope (sailing rubber / rope) was used.

oscilloscope (Voltcraft DG Scope 20 MHz), triggered on the photo interrupter signal. Figure 1b shows the plate (black detection rim) and the photo interrupter. Figure 3 shows the built in detector.

Projectiles and samples

For testing and validation we used projectiles modeled of metal chips (7 g) and fragments with approximate dimension of 10 mm × 15 mm (Figure 4). The projectiles were adapted with a foamed polystyrene insert for alignment in different orientations (Figure 5). Samples were standard occupational safety spectacles mounted on a test head, as seen in Figure 6.

Test procedure

Figure 5 shows the situation before starting with the fixed hinge into the carriage, locked by a splint. After hooking the Bowden cable into the carriage, the projectiles can be loaded. To activate the launching platform and the carriage, we used a long cable for remote control. A Bowden cable out of gummed counter rope (sailing rope) with a thickness of 6 mm results in speed up to 25 m·s⁻¹ (slow velocity, Figure 3), 40 m·s⁻¹ could be reached with two additional ropes on both sides and



Figure 5. Test procedure with two natural tube rubbers (14.4 mm / 4.8 mm). The carriage was load with a metal object, adapted with a foamed polystyrene insert. The starting arm with the fixed hinge into the carriage is locked by a splint.

an entire span length of 25 m (medium velocity). Additionally we used two or four natural tube rubbers with a thickness of 14.4 mm (4.8 mm inner tube) for high velocities. For example, the setup reaches about 350 N drag force with a 600% pretension on four tube rubbers. With a carriage weight of 128 g + 7 g including metal parts and projectile, velocities up to 62 ± 2 m·s⁻¹ could be reached. For evaluation, we used a monochrome high speed camera with 58 fps (iDS GigE uEye UI-5220-M-DL, max. 100 fps) to analyze the projectile impact on the spectacle. For slow motion analysis, the entire setup was filmed by a Sony HD cam (Sony HDR-CX115EL Full



Figure 4. Metal projectiles for impact tests (left: not deburred; right: approx. 10 mm × 15 mm sloped round bar).

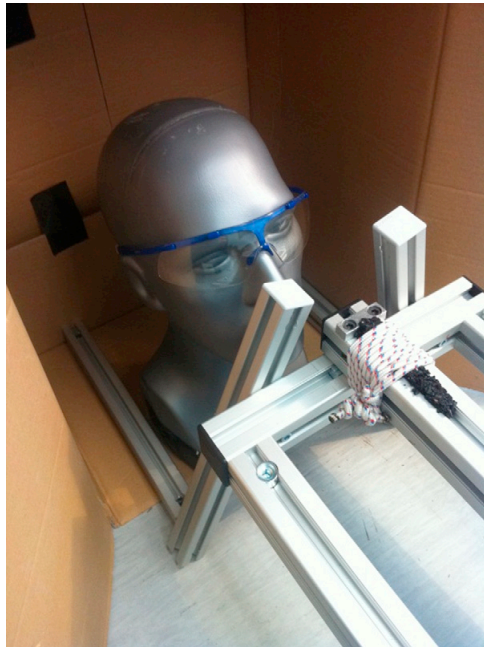


Figure 6. Launching platform aligned on a head, wearing an occupational safety spectacle.

HD Camcorder). The goggle samples were inspected visually for damage penetration test.

Results

For repeatability test, we performed repeat measurements with the same projectile loaded the launching platform two times and shot on the same sample with the same insert and alignment. The deviation of both impacts was approximately 1 mm on the spectacle surface, with a free flight distance of about 150 mm (launching platform end to the spectacle surface).

We performed impact tests with slow, medium and high speed projectiles. All tests with velocities from $10 \text{ m}\cdot\text{s}^{-1}$ up to $62 \text{ m}\cdot\text{s}^{-1}$ fired the spectacle off the test head. The spectacles transformed the kinetic energy into ductile and compressible deformation, without projectile contact to the eye. The first run with full cable load, empty carriage and single – row 6 mm gummed sailing rope reached $26 \text{ m}\cdot\text{s}^{-1}$. A velocity of $36 \pm 2 \text{ m}\cdot\text{s}^{-1}$ could be reached in the second medium speed run with charged carriage. The projectile, adjusted with the flat parts in direction of flight, hit the polycarbonate with an edgeless flank and due to the impact one side of the frame was broken. For the high speed test, the projectile was aligned with the sharp edge ahead. With a velocity of $62 \pm 2 \text{ m}\cdot\text{s}^{-1}$, achieved

with four prestressed natural tube rubbers (14.4 mm), the impact caused a crack into the polycarbonate without surface penetration.

Discussion

Occupational material machining and processing often causes eye injuries with high speed mostly natural foreign bodies. Eye protection devices such as safety spectacles and shields are important for protecting the eye from severe injury. Regulations and standards are defined in DIN EN 166 and ANSI Z 87.1 [4,5]. The regulations only refer to protective effect in a standardized test setup with bullets or missiles. However, the requirements do not refer to tests for small heavy objects with arbitrary shape or mass and do not differentiate between projectiles like slivered glass or blunt / sharp metal particles. To have full flexibility of particles speed, shape and weight, we built up an experimental test setup for assessment of impact resistance for occupational eyewear against high velocity objects. With this system, we were able to accelerate objects up to $62 \pm 2 \text{ m}\cdot\text{s}^{-1}$ and to direct these objects to a test head, wearing an eye protection device. The setup allows using a variety of projectile shapes (up to $30 \text{ mm} \times 30 \text{ mm} \times 40 \text{ mm}$), velocities from minimum $2 \text{ m}\cdot\text{s}^{-1}$ to $62 \text{ m}\cdot\text{s}^{-1}$ and different orientation of the particles in direction of flight. The impact could be analyzed by a high speed camera for slow-motion. The accuracy of measurement was $\pm 2 \text{ m}\cdot\text{s}^{-1}$ for high velocity and the aiming accuracy was about 1 mm (impact deviation on the spectacle surface of two shots). Comparison with the literature shows that common setups can be equipped only with one specialized type of particles like missiles, slugs, rimfire projectiles, pellets or balls in a defined orientation [8,10,12]. Typical velocities were from $38 \text{ m}\cdot\text{s}^{-1}$ to $185 \text{ m}\cdot\text{s}^{-1}$, $152 \text{ m}\cdot\text{s}^{-1}$ or $290 \text{ m}\cdot\text{s}^{-1}$ in comparison to our actual limit of $62 \text{ m}\cdot\text{s}^{-1}$ [10,13,14].

For setup validation we used standard occupational safety eyewear and projectiles, such as metal shiver and fragments with approximate dimension of $10 \text{ mm} \times 15 \text{ mm}$ with velocities from $10 \text{ m}\cdot\text{s}^{-1}$ up to $62 \text{ m}\cdot\text{s}^{-1}$. The impact test with $36 \pm 2 \text{ m}\cdot\text{s}^{-1}$ broke one side of the spectacle frame off. Another test with $62 \pm 2 \text{ m}\cdot\text{s}^{-1}$ cracked the polycarbonate shield, but without any contact to the “eye” of the test head. We suppose that the spectacles could protect from higher velocities, before the projectile penetrates the polycarbonate shield or causes mature cracks through the entire shield. For example, studies showed ballistic limits of about $100 \text{ m}\cdot\text{s}^{-1}$ for optic lenses (CR-39), $210 \text{ m}\cdot\text{s}^{-1}$ for polycarbonate spectacles and $204 \text{ m}\cdot\text{s}^{-1}$ for polycarbonate goggles [10,13].

Limitations

All tests were performed with standardized occupational safety eyewear, which comply with the requirements of DIN EN 166 [5]. The normative requirements for spectacles only refer to a minimum resistance tested with a 22 mm steel

bullet and a force of 100 ± 2 N, a higher resistance with a bullet mass of 43 g and $5.1 \text{ m}\cdot\text{s}^{-1}$ speed and (DIN EN 168) requirements for high speed bullets with 0.86 g mass and a velocity of $45 \pm 1.5 \text{ m}\cdot\text{s}^{-1}$ [6]. But there is no information about protection capabilities against large and heavy arbitrary objects or any recommendation for its applications (in which case the spectacle is to use).

A limitation refers to the material stress. With the current setup the speed of the foreign bodies is limited to around $60 \text{ m}\cdot\text{s}^{-1}$. We did not study the long-term stability of the carriage material in term of abrasion on the elastic bands. Due to the high force on the base unit, a slight drift of the entire setup on the ground could not be fully excluded. Such a movement could slightly falsify the speed measurement.

Further work will address carriage optimization, electric ignition and higher velocity. We plan to test wear resistant materials with lower friction and good sliding effects. The maximum weights of the carriage and the Bowden cable mass have to be reduced in order to gain test velocities. For further studies with hazardous projectiles, a wireless ignition has to be developed.

Conclusion

In conclusion, we created a test setup for impact resistance test for occupational eyewear. The setup can be applied for investigation on ophthalmic trauma caused by foreign body intrusion e.g. injury reconstruction or material testing with standardized and non-standardized projectiles.

References

- [1] Hauptverband der gewerblichen Berufsgenossenschaften e.V. BGV A1 Grundsätze der Prävention. In: Berufsgenossenschaftliche Vorschrift für Sicherheit und Gesundheit bei der Arbeit. HVBG Hauptverband der gewerblichen Berufsgenossenschaften; 2004.
- [2] Hod Y, Geyer O. Eye injuries caused by rotating wire brushes. *Harefauh: J Isr Med Assoc* 2005;30:4:239–40.
- [3] Mackiewicz J, Machowicz-Matejko E, Salaga-Pylak M, Piecyk-sidor M, Zagorski Z. Work - related, penetrating eye injuries in rural environments. *Ann Agric Environ Med* 2005;12:27–9.
- [4] Standard ANSI Z 87.1 2003 Occupational and educational personal eye and face protection devices – spectacles.
- [5] Standard DIN EN 166 2001 Personal eye protection - Specifications.
- [6] Standard DIN EN 168 2001 Personal eye-protection - Non-optical test methods.
- [7] Wigglesworth E. A ballistic assessment of eye protector lens materials. *Invest Ophthalmol Vis Sci* 1971;10:985–91.
- [8] Chou B, Gupta A, Hovis J. The Effect of Multiple Antireflective Coatings and Center Thickness on Resistance of Polycarbonate Spectacle Lenses to Penetration by Pointed Missiles. *Optometry Vision Sci* 2005;82:964–9.
- [9] Choi BR, Yuen GS-C, Dain SJ. Ballistic impact resistance of selected organic ophthalmic lenses. *Clin Exp Optom* 2011;94:568–74.
- [10] Rychwalski P, Packwood EA, Cruz O, Holds J. Impact Resistance of Common Spectacle and Safety Lenses to Airgun and Rimfire Projectiles. *J AAPOS* 2003;7:268–73.
- [11] Uchio E, Ohno S, Kudoh J, Aoki K, Kisielewicz L. Simulation model of an eyeball based on finite element analysis on a supercomputer. *Brit J Ophthalmol* 1999;83:1106–11.
- [12] Oliver A, Chou B. A Ballistic Evaluation of the Impact Resistance of Spectacle Lens Materials. *Optometry Vision Sci* 1993;70:822–7.
- [13] Goldsmith W. Projectile impact on glass and polymeric ophthalmic lenses and circular plates. *Am J Optom Physiol Opt* 1974;51:807–31.
- [14] Welsh KW, Miller JW, Kislin B, Tredici TJ, Rahe AJ. Ballistic impact testing of scratched and unscratched ophthalmic lenses. *Am J Optom Physiol Opt* 1974;51:304–11.

Available online at www.sciencedirect.com

SciVerse ScienceDirect

4 Veröffentlichung 2

Inspection of freeform intraocular lens topography by phase measuring deflectometric methods

Alexis Speck,^{1,*} Benedikt Zelzer,¹ Marc Kannengießer,¹
Achim Langenbucher,^{1,2} and Timo Eppig¹

¹Experimental Ophthalmology, Saarland University, Kirrberger Strasse 100, Homburg/Saar 66424, Germany

²SAOT Erlangen Graduate School of Advanced Optical Technologies, Paul-Gordan-Strasse 6, Erlangen 91052, Germany

*Corresponding author: alexis.speck@uks.eu

Received 3 April 2013; revised 16 May 2013; accepted 17 May 2013;
posted 20 May 2013 (Doc. ID 188200); published 18 June 2013

Manufacturing spherical, aspheric, and freeform surfaces requires testing throughout the development and production process. State-of-the-art topography measurement is limited in applicability for intraocular lenses (IOLs), and there is no dedicated commercial surface measurement system available for freeform IOLs. The purpose of this work was to validate a deflectometric setup for surface measurement, detection of defects, and shape fidelity analysis for the development and production of IOLs. The setup is based on a phase measuring deflectometer with a field-of-view of 80 mm × 80 mm and a mean repetition accuracy of $1.6 \cdot 10^{-3}$ D. The technique is suitable for detection of global and local surface errors, extracted from geometry and topography analysis. For validation according to DIN ISO 5725:2002, spherical IOLs with radii of curvature of 10 and 20 mm, a commercial aspheric IOL, and single-sided freeform IOL samples were used. © 2013 Optical Society of America

OCIS codes: (120.0120) Instrumentation, measurement, and metrology; (170.0170) Medical optics and biotechnology; (230.0230) Optical devices; (240.0240) Optics at surfaces; (350.0350) Other areas of optics; (040.1490) Cameras.

<http://dx.doi.org/10.1364/AO.52.004279>

1. Introduction

Cataract is a very common ocular disease in which the crystalline lens of the eye becomes cloudy. It is one of the most frequent causes of loss of vision, and most cataracts occur in the aging eye, whereas other cataract forms are caused by accidents, other ocular diseases, or medication. The treatment of a cataractous eye involves removal of the crystalline lens and implantation of an artificial intraocular lens (IOL). In addition, IOLs are often used for refractive correction of the eye as an alternative to laser refractive surgery. Currently available IOLs simply provide defocus correction or additionally correct astigmatism (toric IOLs) or spherical aberration (referred to as aspheric IOLs). Correction of other higher-order aberrations requires customized IOLs with freeform

surfaces [1,2]. These surfaces, described by polynomials, have to be cross checked during manufacturing processes. Available methods for noncontact topography measurement of IOLs are limited due to the small sample dimensions and delicate handling requirements. Several methods have been introduced for measuring IOL topography. Atomic force microscopy was used to analyze the surface of commercially available IOLs. In this study, four IOL surfaces were measured with high resolution in a nanometer range. In comparison, the complex measurements were made in a liquid environment (with contact) [3,4]. In another study, three clinical topographers were used and handling and technical specifications, e.g., resolution, accuracy, and repeatability, were assessed [5]. The measurement principles were based on Placido rings, Scheimpflug imaging, and optical coherence tomography (OCT). Only the Placido system under test (Tomey TMS-2N) proved to be an appropriate measuring device,

limited to a range of radii of curvature (ROCs) between 8 and 13.5 mm. There are several systems on the market, such as the WaveMaster Reflex (Trioptics GmbH, Wedel, Germany), the SHSOphthalmic autoROC (Optocraft GmbH, Erlangen, Germany), and the Kaleo-R IOL (Phasics S.A., Palaiseau, France), which are based on a non-null test using a Shack-Hartmann sensor or other wave-front sensing techniques in the reflection mode for measuring IOLs or contact lenses [6–9]. Most other commercial devices specialized for the IOL industry are designed for functional measurement in transmission, such as the OptiSpheric and the WaveMaster (Trioptics), the SHSOphthalmic (Optocraft), PMTF and NIMO 0815 (Lambda-X sa, Nivelles, Belgium), Kaleo-I (Phasics), or the IOLA series [Rotlex (1994) Ltd., Omer, Israel] [7,8,10–16]. The systems are designed to measure spherical, aspherical, toric, or multifocal toric lenses in the transmission mode. The CURV (Lambda-X) is based on Placido rings and measures ROCs between 6 and 25 mm with an accuracy of $\pm 10 \mu\text{m}$ [17]. Other optical techniques for laboratory tests are based on wave-front sensing, OCT, and interferometric or imaging-based techniques [18–21].

To our knowledge, there is no published study on the application of phase measuring deflectometry (PMD) for measurement of (single-sided, semifinished) freeform IOL surfaces. However, this technology is already established in ophthalmic optics for measurement of progressive spectacle and lens surfaces. The advantages are direct measurement of surface slopes and optical power and monitoring of lens cosmetics and cleanliness [22,23]. In this study we applied a deflectometric measurement setup for measuring the topography of spherical, aspherical, and freeform IOLs. The purpose of this study was to validate the system for measuring the entire surface and detection of defects for the production of IOLs.

2. Material and Methods

Our setup is based on a deflectometer (Schneider GmbH & Co.KG, Fronhausen, Germany) equipped with two cameras. The cameras ($f' = 16 \text{ mm}$) are used for absolute position measurement in space (standardized PMD sensor) with a field-of-view (FoV) of $80 \text{ mm} \times 80 \text{ mm}$, designed for a typical spectacle glass before glazing. The system is specified for measuring higher reflective surfaces. The extraction of geometry and topography is based on slope data (raw format). For retrieval of height and curvature data, the results have to be integrated or differentiated. A mean repetition accuracy of $1.6 \cdot 10^{-3} \text{ D}$ is specified when measuring within a working range of concave radius $r = -40 \text{ mm}$ to $-\infty$ and convex radius $r = 40 \text{ mm}$ to ∞ [24]. These radii are considerably flatter than the ROCs typically used in IOLs (~ 7 – 35 mm). For our IOL tests, we performed accuracy and repeatability tests with spherical IOLs with ROCs of 10 and 20 mm. We acquired a set of six measurements for each test after calibration of the system. Additionally, we performed tests with

a commercial aspherical IOL (AF-1 NY-60, Hoya Surgical Optics, Tokyo, Japan) with a nominal power of 24.50 D (Fig. 2). Analysis of the surface data was assisted by GOM Inspect (GOM mbH, Braunschweig, Germany) and SoftPMD (Max Planck Research Group, OSMIN, Friedrich-Alexander-University of Erlangen-Nuremberg, Germany) software packages. Analysis of spherical IOLs was performed by subtraction of predefined-, best-fit spheres and inspection of the mean ROC. Global shape differences and local surface quality were presented in color-coded plots.

A. Accuracy and Repeatability Testing

For measurement error examination, curvature and height data were used. Twelve measurements were acquired consecutively using identical parameters. For repeat accuracy (first series), the sample was aligned in a constant position, and for the repeatability test (second series), the sample was aligned six times in different arbitrary positions in space. For the lateral field, the same circular aperture was used to crop the optic part from the whole image. We analyzed the accuracy through the systematic error of measurement (bias of the measuring instrument), the repeatability through the standard deviation (SD) of a series of the repeated measurements, and the stability according to DIN ISO 5725:2002 [25].

We compared the mean values and mean differences of the measurements of the second series. Additionally, we performed all comparisons with the curvature data of the samples. Due to the software algorithm, a direct calculation of the radius was not possible. Therefore we had to transform the data provided by software with a fictive refractive index of $n = 2$ to surface powers, as the software automatically uses $n = 1$ for the surrounding medium. Power in balanced saline solution ($n_s = 1.336$, similar to the aqueous humor of the human eye) was additionally derived.

The curvature and the surface mean power were calculated by differentiation of the slope data. The ROC was extracted on an unweighted reciprocal average of the deviation of slope data measurement within the region of interest (ROI). With a mean radius and a design radius r_{design} of 10 mm, the bias (systematic error) could be calculated [Eq. (1)]. Power in saline P_s was calculated with a refraction index of 1.336 for balanced saline solution and the refractive index of the lens material [Eq. (2)]:

$$\text{bias} = |\bar{r} - r_{\text{design}}|, \quad (1)$$

$$\text{Power in saline } P_s = \frac{n_s}{f} = \frac{n_s \cdot (n_{\text{IOL}} - n_s)}{n_s \cdot r}; \quad \frac{1}{f} = \frac{n' - n}{n \cdot r}$$

with

$$n_{\text{IOL}} = 1.492,$$

$$n_s = 1.336. \quad (2)$$

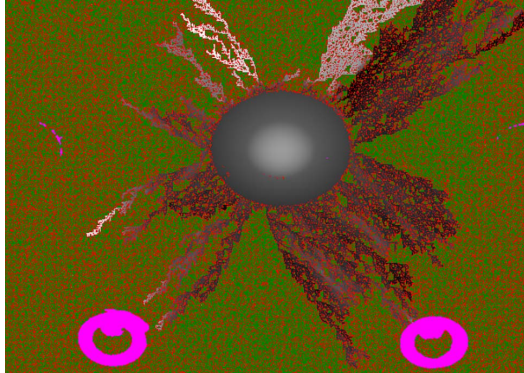


Fig. 1. Measurement of a spherical IOL with an ROC of 20 mm. The entire measurement field with 1280×960 pixel camera resolution was used. The measured IOL surface is marked in gray color (bright, optical part; dark, haptic). The outer and biggest part of the IOL is later used for the haptic. Overexposed regions in the FOV are colored in pink.

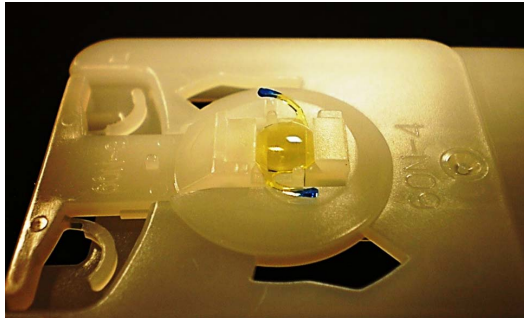


Fig. 2. Commercial aspherical IOL HOYA AF-1 NY-60 with a blue blocker and a power of 24.50 D.

B. Samples

We measured 12 spherical IOLs made of polymethylmethacrylate ($n \approx 1.492$) with an ROC between 10 and 20 mm and an optic diameter of 6 mm. One side of the IOLs was blocked with wax on a special holder for the turning machine. The surface was described by fitting the height design data to the measured surface and showing the residuals. Only the optical

part of the IOL was used for examination (center part of the whole image in Fig. 1).

For aspheric and freeform surfaces, we evaluated six IOLs with predefined higher-order aberrations (e.g., defocus, astigmatism, and tilt). Three individually shaped freeform IOLs designed to compensate for optical aberrations of a real eye (customized IOL) were evaluated. Additionally a rotationally symmetric aspheric IOL Hoya AF-1 NY-60 was used to show the applicability with a real aspheric IOL (Fig. 2). The optics diameter is about 6 mm, and the overall diameter is 12.5 mm. The aspheric profile is located on one surface only, which is constant for a wide range of available powers (power adjustment is done by customization of the second surface). As a working example, we used a lens power of 24.50 D. For analysis, the aspherical surface design data (personal communication, Hoya Corp.) were subtracted from the measured mesh to point out local deviations from the target shape.

3. Results

Table 1 shows the accuracy measurement data with a spherical IOL ($ROC = 10$ mm). The difference between target and measurement is provided in terms of range, mean, and SD. The results were not smoothed, especially not the spikes and the outlier. The maximum values were from $-1.5 \mu\text{m}$ to about $1 \mu\text{m}$ with a peak to valley (PV) of $2.6 \mu\text{m}$. With a mean radius and a design radius r_{design} of 10 mm, the bias (systematic error) could be calculated, and it resulted in a systematic error of measurement of about $13 \mu\text{m}$:

$$\begin{aligned} \text{bias} &= |\bar{r} - r_{\text{design}}| \quad \text{with } r_{\text{design}} = 10.0 \text{ mm}, \\ \bar{r} &= 9.987 \text{ mm}, \quad \text{and} \quad \text{bias} \approx 13 \mu\text{m}. \end{aligned} \quad (3)$$

Table 2 shows the respective data with the repeat measurement series V7 to V12. SD indicates the repeatability of the measurement setup. In particular, the measurement with the highest outlier resulted in a distance range (PV) of about $1.5 \mu\text{m}$. An averaging filter for the outlier and spikes was not used. This series resulted in higher deviations, due to our nonreferenced method with free lateral field and free positioning in the coordinate system. The

Table 1. Accuracy Measurement with a Spherical IOL with $ROC = 10$ mm

Definition	Measurements	ID	Accuracy																		
			Error	Unit	V1	V2	V3	V4	V5	V6	Max-Min	Mean	SD	Median							
Range (PV)	[μm]		2.627		1.715		1.288		1.472		1.011		1.201		1.616		1.552		0.528		1.380
Mean	[μm]		0.138		0.111		0.101		-0.020		-0.015		-0.008		0.158		0.051		0.066		0.046
SD	[μm]		0.580		0.356		0.272		0.304		0.209		0.243		0.372		0.327		0.122		0.288
Curvatures			V1_c		V2_c		V3_c		V4_c		V5_c		V6_c								
Mean power P	[D]		100.9		100.5		100.3		99.5		99.7		99.6		1.4		100.1		0.51		100.1
Mean radius " r_i "	[mm]		9.91		9.95		9.97		10.05		10.02		10.03		0.14		9.987		0.05		10.00
P_s	[D]		15.7		15.7		15.7		15.5		15.6		15.6		0.2		15.6		0.08		15.6

Table 2. Repeatability Measurement with a Spherical IOL with ROC = 10 mm

Definition	Repeat Measurements	Repeatability												
		Error	Unit	V7	V8	V9	V10	V11	V12	Max—Min	Mean	SD	Median	
Range (PV)	[μm]	1.078		1.024		1.072		0.870	1.225	5.184	4.314	1.742	1.543	1.075
Mean	[μm]	-0.024		-0.025		-0.026		0.010	0.003	0.024	0.051	-0.006	0.020	-0.010
SD	[μm]	0.227		0.207		0.221		0.156	0.266	1.376	1.220	0.409	0.434	0.224
Curvatures		V7_c		V8_c		V9_c		V10_c		V11_c		V12_c		
Mean power P	[D]	99.9		99.75		99.7	100.0	99.6	97.6	2.4	99.4	0.85	99.8	
Mean radius “ r_i ”	[mm]	10.00		10.02		10.02	10.00	10.04	10.25	0.25	10.05	0.09	10.02	
P_s	[D]	15.6		15.6		15.6	15.6	15.6	15.2	0.4	15.5	0.13	15.6	

Table 3. Analysis of the Spherical IOL Topographies

Definition	Sample																
	Sample No.	design	ROC	error	Unit	1	2	3	4	5	6	7	8	9	10	11	12
Min					[mm]	15.5	20	16	18	14.5	14	10	15	13.5	13	12.5	12
[μm]					[μm]	-5.89	-0.26	-8.19	-0.15	-1.56	-0.92	-0.46	-0.23	-1.35	-0.47	-4.04	-1.06
Max					[μm]	5.91	0.20	7.54	0.23	0.79	0.62	0.46	0.45	1.59	0.48	4.18	1.91
Range					[μm]	11.808	0.470	15.738	0.387	2.352	1.551	0.933	0.683	2.947	0.961	8.231	2.988
Mean					[μm]	0.22	0.034	0.34	0.03	0.15	0.10	0.02	-0.02	-0.01	-0.01	-0.06	0.01
SD					[μm]	2.110	0.099	4.221	0.073	0.494	0.314	0.145	0.093	0.752	0.187	1.161	0.526

range is about 1.3 μm higher than the specified measurement uncertainty.

The measurement series with an ROC of 20 mm resulted in a systematic error of measurement of 2 μm , calculated with the design radius $r_{\text{design}} = 20$ mm and the extracted bias (systematic error) from the curvature data. The PV of the residuals and the accuracy check were below 1 μm . The stability was about 600 nm.

A. Sample Measurements

Table 3 illustrates the spherical IOL samples. Figure 3 shows an example of a deviation plot (color-coded) and cross section for an ROC of 20 mm. The design ROC was provided by the manufacturer. Min, max, range (PV), mean, and SD characterize the differences of the measurement from the target design. Samples 1 and 3 showed large PV of about 12 and 16 μm , due to a scratch over the whole surface.

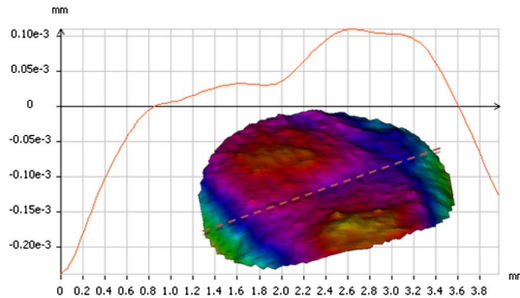


Fig. 3. Deviation of the spherical IOL with an ROC of 20 mm and a spherical fit. The cross section is shown along the dashed line. The measurements were not smoothed.

The SD of both samples represented the error with higher values of 2 and 4 μm . Samples 5, 8, 10, and 12 showed homogeneous global variations, indicated by moderate mean and SD values. The theoretical radius (target shape) did not fit at all to the measurement, due to a constant offset (larger or smaller mean radii). The other samples yielded only a deviation in a micrometer range from the target design.

Figure 4 represents the color-coded plots of the freeform IOLs F1 to F3. Comparison of the measurement with the design data demonstrated the expected form variation, e.g., defocus or astigmatism of the surfaces. In Table 4 the statistics of samples T1 to T6 and F1 to F3 are provided. T1 to T6 show precalculated higher freeform fractions, and F1 to F3 are full freeform shapes as represented in Fig. 4.

Figure 5 illustrates a deviation plot of one side of the commercial Hoya IOL. The design data were represented by polynomials of fourth- and fifth-order. Local deviations were within a micrometer range. The histogram marks the distribution of the deviation.

4. Discussion

We applied a deflectometric setup for measuring freeform IOL topographies. The PMD sensor is typically used for specular surfaces, such as glass and lens materials. Application fields of the deflectometer are window shields, bodyworks, and mold production [26–28], typically with large samples to be measured. The PMD technique has already been established for quality control and evaluation of toric and progressive optics [23]. To our knowledge, there are no published results for measuring IOL topographies with PMD. To test the applicability of

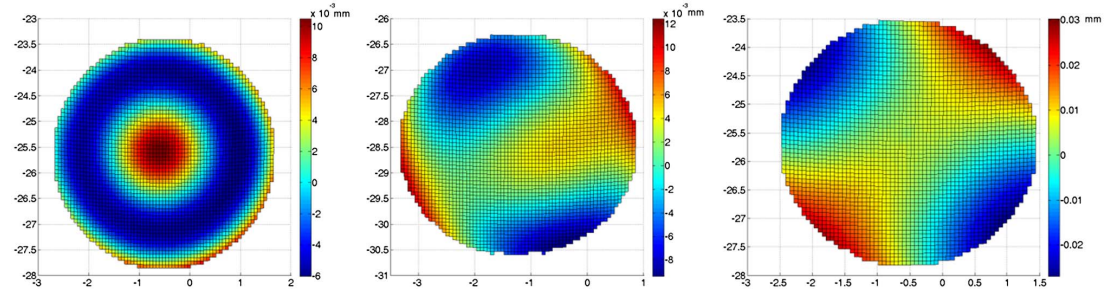


Fig. 4. False color plots of the F1 to F3 freeform IOL target versus actual comparison (from left to right).

the technique and validate the system for surface examination, detection of defects with outwears, and measurement of the ROC, we evaluated 22 IOLs with 52 measurements. The samples' ROCs ranged from 10 to 20 mm for the spherical forms. Additionally, we used samples with higher-order aberrations and freeform samples with known aberrations. For a commercial example, we used a common aspheric IOL with an optics diameter of about 6 mm and an optical power of 24.50 D.

The analysis of the surfaces was based on actual versus target comparison. The design data were subtracted from the measured shapes and presented as deviation plots, curvature maps, and height data maps for further analysis. For accuracy and repeatability test, we used IOLs with ROCs of 10 and 20 mm. The bias, with respect to the systematic error of the measuring instrument, is 13 μm for the 10 mm IOL. For repeatability, the SD of the measurements was about 1.5 μm . The PV value was 4 μm between six repeat measurements (about 10 mm with outlier). The stability of the system is 1.5 μm in the accuracy test and 1.7 μm in the worst-case scenario. This indicates a good accuracy, due to the small IOL radius and the large measurement field in comparison to the specified measurement uncertainty of about 3 μm for the specified lateral measurement range (80 mm). For measuring these small IOL radii, the maximum values of $-1.5 \mu\text{m}$ to about 1 μm (PV of 2.6 μm) confirmed the accuracy. For the repeatability test, the device under test was aligned six times in different positions in space. Due to the arbitrary positioning and the analysis method (crop out the optical area to define the ROI), each measurement was acquired in a different absolute position in space.

Nevertheless, we used the same parameters and only had to reposition the cropped area for the analysis. We believe a blocker or mounting device for the IOL, as is usually used for such tests, might improve the repeatability of the technique.

The accuracy calculation from the curvature measurement resulted in a maximum deviation of 9 μm for the accuracy and 25 μm for the repeatability series. The measurement series with an ROC of 20 mm resulted in a systematic error of measurement of 2 μm , calculated with the design radius $r_{\text{design}} = 20 \text{ mm}$ and the extracted bias (systematic error) from the curvature data. The PVs of the residuals and the accuracy check were below 1 μm . The stability was about 600 nm. As expected, the accuracy with the 20 mm IOL was better than the test with the 10 mm ROC. We suppose the accuracy is worse with smaller a ROC due to large angles of incidence on the sample surface.

Quantitative evaluation of spherical, aspherical, and freeform samples was successful. The spherical samples (1 and 3) had PVs of about 12 and 16 μm , due to a scratch over the surface. We suppose these defects occurred during the production process or due to handling and transport. The higher SD of up to 4 μm confirmed the error. Various samples (5, 8, 10, and 12) showed a homogeneous and smooth surface. Low average and SD values over the entire deviation plot conducted high shape fidelity. Leftovers resulted in local form deviations in a micrometer level. The expected and precalculated surface data of the measured aspheric and freeform IOLs could be resampled. A comparison of the measurements and the design data extracted the expected shapes, e.g., defocus or astigmatism. We also calculated and

Table 4. Analysis of the Freeform IOL Topographies

Error	Unit	Samples								
		T1	T2	T3	T4	T5	T6	F1	F2	F3
Min	[μm]	-2.500	-0.950	-1.184	-0.682	-5.474	-5.882	-6.132	-10.607	-30.266
Max	[μm]	1.806	1.506	1.489	0.918	2.757	9.979	10.805	11.582	32.594
Range	[μm]	4.306	2.457	2.674	1.600	8.231	15.862	16.936	22.189	62.860
Mean	[μm]	-0.023	-0.069	0.015	0.012	0.048	-0.237	-1.078	0.473	0.703
SD	[μm]	0.617	0.466	0.514	0.281	0.767	0.651	4.301	4.784	12.960

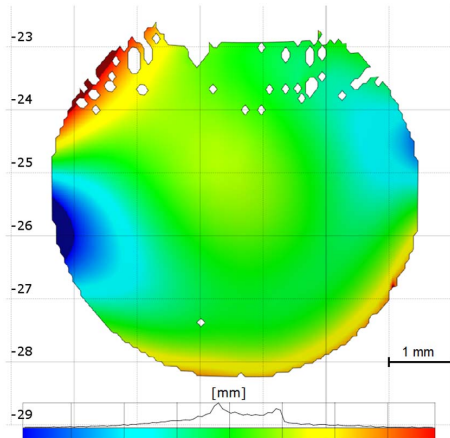


Fig. 5. Deviation plot of the commercial aspherical IOL Hoya AF-1 NY-60. Fitted design data was subtracted from the measured aspheric topography.

subtracted the design data from the IOL surface of a commercial IOL (surface with polynomial of sixth-order). Local deviations were below 1 μm . The measurement system analysis (MSA) was stable. We suppose these measured local deviations do not have any consequences for the patient. Global or local deviations with a higher ratio to the entire IOL surface and errors with some micrometers are much more critical. The measured IOL was checked in another publication, with regard to tilt, decentration, and general misalignment as well [29]. The measured IOL is robust and shows only a slight decrease in image quality. As a matter of fact, form deviations, e.g., 1 μm regardless of type, should not alter the image quality.

A. Limitations

A limitation refers to the MSA. Our analysis was limited to a single operator. Therefore we were unable to perform an interoperator analysis. Also a linearity analysis was not possible, due to the lack of repeat measurements of more than one IOL sample.

The procedure of measuring the commercial IOL was difficult. We had to use an index matching liquid and a black light absorbing ground to eliminate back surface reflections. This method is inefficient and ineligible in a factory, inline measurement or working conditions at all. The alignment of the matching package was sophisticated, due to a bubble-free preparation. Figure 6 illustrates the measurement grid of a Hoya sample. There was air on the upper edge and a smaller bubble in the middle section. The alignment of the IOL on the various matching tests is represented in Fig. 7.

This directly leads to the major limitation for commercial application of the technique. Liquid index matching is not feasible for hydrophilic materials because of diffusion of the fluid into the material. Another point is the contamination of the IOL by

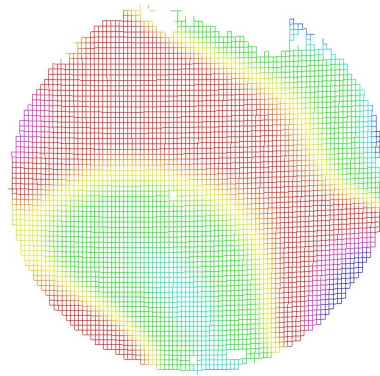


Fig. 6. Measurement grid of the commercial IOL. Note the bad spots due to the blow forming and the fast index matching.

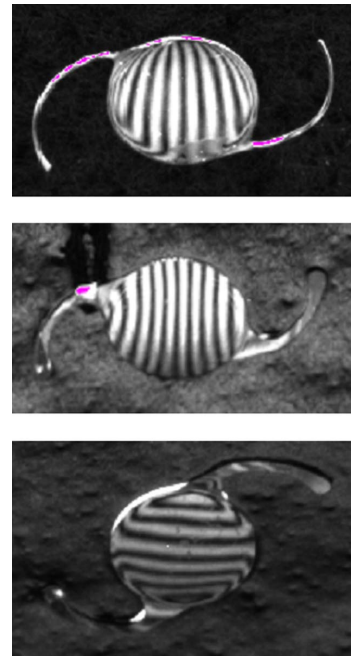


Fig. 7. Deflectometric measurements of the commercial Hoya IOLs. The backsides were aligned on an index matching pad with liquid matching gel. The sinusoidal projected pattern is visible.

the matching liquid, as IOLs have to be handled in a sterile clean room environment.

Therefore the current preparation method is a destructive one—although the measurement technique itself allows nondestructive measurement. This implies only a random inspection was possible between the production processes. A solution to these problems might be a redesign of the technique using UV light. Therefore different sinusoidal pattern sources and optics are required.

Another limitation is related to the resolution of the setup. The setting contains two cameras ($f' = 16$ mm) with a defined distance to the specimen. This results in a measurement field of $80\text{ mm} \times 80\text{ mm}$ and an FoV of 80 mm lateral, which we used for the IOL measurements. Thus, the cameras are not fully exploited due to the fact that the entire field was not used. For example, Fig. 1 shows the whole measurement field. The optical part of the IOL surface was imaged by about 66×66 pixels (of 1280×960 pixels). This results in a usage of 35% of the total measurable field. Better accuracy could be achieved with customized optics.

In comparison, the NIMO RE3004 (Lambda-X) is the equivalent to the PMD sensor and has almost the same application fields, e.g., topology analysis of high gloss surfaces such as mirrors and ophthalmic optics. The device is based on the phase-shifting Schlieren technique, measuring specular reflective surfaces with an absolute accuracy of 0.3%, and is specified for a concave/convex range between ∞ and 200 mm. We suppose radii less than 200 mm could be possible, with a loss of resolution and accuracy. Again, the lateral field has to be adapted with the appropriate optics and working distance for IOLs. The Kaleo-R IOL (Phasics) is specified to measure toric and aspherical IOLs with ROCs between 6 and 35 mm with an absolute precision of better than $10\text{ }\mu\text{m}$ in ROCs.

However, we demonstrated that the accuracy and stability are sufficient for measuring IOLs with PMD. We believe that a customized PMD setup will be competitive with other available techniques. Further work will address studies with optimized blocker and mounting devices. The repeatability results of the setup will be improved through a holding system for IOLs. We also plan to use an optimized camera setting and optics for the small lateral field of an IOL.

5. Conclusion

The PMD technique is a way to measure freeform IOL topographies. An optimization of the setup, e.g., through well-adapted camera lenses with appropriate focal length and an IOL blocking system leading to higher resolution, is necessary in order to achieve higher accuracy and repeatability.

The authors gratefully acknowledge funding by the Bavarian Research Foundation (AZ-874-09).

References

1. A. Langenbucher, T. Eppig, B. Seitz, and E. Janunts, "Customized aspheric IOL design by raytracing through the eye containing quadric surfaces," *Curr. Eye Res.* **36**, 637–646 (2011).
2. Z. Zhu, E. Janunts, T. Eppig, T. Sauer, and A. Langenbucher, "Tomography-based customized IOL calculation model," *Curr. Eye Res.* **36**, 579–589 (2011).
3. M. Lombardo, M. P. De Santo, G. Lombardo, R. Barberi, and S. Serrao, "Analysis of intraocular lens surface properties with atomic force microscopy," *J. Cataract Refract. Surg.* **32**, 1378–1384 (2006).
4. M. Lombardo, S. Talu, M. Talu, S. Serrao, and P. Ducoli, "Surface roughness of intraocular lenses with different dioptric powers assessed by atomic force microscopy," *J. Cataract Refract. Surg.* **36**, 1573–1578 (2010).
5. M. Kannengiesser, Z. Zhu, A. Langenbucher, and E. Janunts, "Evaluation of free-form IOL topographies by clinically available topographers," *Z. Med. Phys.* **22**, 215–223 (2012).
6. J. Pfund, N. Lindlein, J. Schwider, R. Burow, T. Blumel, and K. E. Elssner, "Absolute sphericity measurement: a comparative study of the use of interferometry and a Shack-Hartmann sensor," *Opt. Lett.* **23**, 742–744 (1998).
7. Trioptics GmbH, "Flexible and reliable wavefront measurement," <http://www.trioptics.com/wavemaster/description.php> (accessed 21 February 2013).
8. Optocraft GmbH, "SHSOphthalmic autoROC—Shape and surface testing of intra ocular lenses and contact lenses," <http://www.optocraft.de/products/SHSautoROC/index.en.php> (accessed 21 February 2013).
9. S. A. Phasics, "Kaleo-R IOL: Surface characterization for ophthalmologic lenses industry," <http://www.phasicscorp.com/products/kaleo-range/kaleo-r-iol.html> (accessed March 2013).
10. Trioptics GmbH, "OptiSpheric—the industry's standard for lens testing. Product sheet," http://www.trioptics.de/pdfs/OptiSpheric_E_2006.pdf (accessed March 2013).
11. LAMBDA-X, "NIMO TR0815—refractive intraocular lens power mapper and wavefront analyzer. Product sheet," <http://www.lambda-x.com/documents/LX-TR0815.pdf> (accessed 3/2013).
12. Rotlex (1994) Ltd., "Introducing the IOLA PLUS lens analyzer," <http://www.rotlex.com/IolaPlus.asp> (accessed 21 February 2013).
13. Rotlex (1994) Ltd., "IOLA—Introducing the IOLA MultiFocal. Product sheet," <http://www.rotlex.com/IolaMF.asp> (accessed February 2013).
14. S. A. Phasics, "Kaleo-i: Complete and fast accurate IOL quality control," <http://www.phasicscorp.com/products/kaleo-range/kaleo-i.html> (accessed 3/2013).
15. T. Eppig and A. Langenbucher, "Measurement systems for intraocular lenses. Part I—A comprehensive overview on techniques and devices," in *Global CONTACT* (MediaWelt GmbH, 2011), pp. 36–39, <http://de.calameo.com/read/0001260654f441abc6333>.
16. L. Joannes, T. Hough, X. Hutsebaut, X. Dubois, R. Ligot, B. Saoul, P. Van Donink, and K. DeConinck, "The reproducibility of a new power mapping instrument based on the phase shifting Schlieren method for the measurement of spherical and toric contact lenses," *Cont. Lens Anterior Eye* **33**, 3–8 (2010).
17. Lambda-X SA, "CURV—Radius of curvature. Product sheet," <http://www.lambda-x.com/documents/LX-CURV.pdf> (accessed 8 March 2013).
18. T. Eppig, M. Gillner, Z. K. J. Jäger, A. Löffler, and A. Langenbucher, "Biomechanical eye model and measurement setup for investigating accommodating intraocular lenses," *Z. Med. Phys.* **23**, 144–152 (2013).
19. E. Acosta, S. Chamadoira, and R. Blendowske, "Modified point diffraction interferometer for inspection and evaluation of ophthalmic components," *J. Opt. Soc. Am. A* **23**, 632–637 (2006).
20. T. Eppig, K. Scholz, and A. Langenbucher, "Assessing the optical performance of multifocal (diffractive) intraocular lenses," *Ophthalmic Physiol. Opt.* **28**, 467–474 (2008).
21. W. Boucher, S. Velghe, B. Wattellier, and D. Gatinel, "Intraocular lens characterization using a quadri-wave lateral shearing interferometer wave front sensor" *Proc. SPIE* **7102**, 71020Q (2008).
22. M. C. Knauer, C. Richter, O. Hybl, J. Kaminski, C. Faber, and G. Häusler, "Deflectometry rivals interferometry—Deflektometrie macht der Interferometrie Konkurrenz," *Tm.Tech. Mess.* **76**, 175–181 (2009).
23. M. C. Knauer, J. Kaminski, and G. Häusler, "Phase measuring deflectometry: a new approach to measure specular free-form surfaces," *Proc. SPIE* **5457**, 366–376 (2004).
24. Schneider GmbH & Co.KG, "PMD 100-T—Phase measuring deflectometry," <http://www.schneider-om.com/en/products/>

- [ophthalmics/measuring/pmd-100-t.html](#) (accessed 21 February 2013).
- 25. A. Schulze and E. Dietrich, "Statistical methods for machine and process qualification," Carl Hanser Verlag GmbH & CO. KG (2009).
 - 26. S. Kammel, "Deflectometrical analysis of specular reflecting free form surfaces," Ph.D. thesis (Universitätsverlag Karlsruhe, 2005).
 - 27. A. Speck, B. Zelzer, A. Langenbucher, and T. Eppig, "Deflectometry for surface inspection and shape fidelity analysis for manufacturing and polishing of safety spectacle molds," *DgaO Proc.* **113**, 30 (2012).
 - 28. B. Zelzer, A. Speck, A. Langenbucher, and T. Eppig, "Theoretical model for design and analysis of protective eyewear," *Z. Med. Phys.* **23**, 120–128 (2013).
 - 29. M. Gillner, A. Langenbucher, and T. Eppig, "Investigation of the theoretical image quality of aspheric intraocular lenses by decentration. Hoya AF-1 iMics1 und Zeiss ASPHINA (Invent ZO)," *Ophthalmologe* **109**, 263–270 (2012).

5 Veröffentlichung 3

Theoretical model for design and analysis of protectional eyewear

B. Zelzer^{1,*}, A. Speck¹, A. Langenbucher^{1,2}, T. Eppig¹

¹Experimental Ophthalmology, Saarland University, Germany

²SAOT Erlangen Graduate School in Advanced Optical Technologies, Erlangen, Germany

Received 2 August 2012; accepted 5 February 2013

Abstract

Introduction: Protectional eyewear has to fulfill both mechanical and optical stress tests. To pass those optical tests the surfaces of safety spectacles have to be optimized to minimize optical aberrations.

Material and Methods: Starting with the surface data of three measured safety spectacles, a theoretical spectacle model (four spherical surfaces) is recalculated first and then optimized while keeping the front surface unchanged. Next to spherical power, astigmatic power and prism imbalance we used the wavefront error (five different viewing directions) to simulate the optical performance and to optimize the safety spectacle geometries.

Results: All surfaces were spherical (maximum global deviation 'peak-to-valley' between the measured surface and the best-fit sphere: 0.132 mm). Except the spherical power of the model Axcont (-0.07 m^{-1}) all simulated optical performance before optimization was better than the limits defined by standards. The optimization reduced the wavefront error by 1% to 0.150 λ (Windor/Infield), by 63% to 0.194 λ (Axcont/Bolle) and by 55% to 0.199 λ (2720/3 M) without dropping below the measured thickness.

Conclusion: The simulated optical performance of spectacle designs could be improved when using a smart optimization. A good optical design counteracts degradation by parameter variation throughout the manufacturing process.

Theoretisches Modell für die Optimierung und Analyse von Schutzbrillen

Zusammenfassung

Einleitung: Augenschutzgeräte müssen Anforderungen an Festigkeit und optische Qualität erfüllen. Um jenen optischen Ansprüchen gerecht zu werden, sollten die Oberflächen der Schutzbrillen zur Minimierung von Abbildungsfehlern optimiert sein.

Material und Methoden: Die Oberflächendaten von drei gemessenen Schutzbrillen wurden jeweils in ein theoretisches Schutzbrillenmodell (vier sphärische Oberflächen) überführt. Die Rückfläche wurde iterativ optimiert, während die Vorderfläche beibehalten wurde. Neben den optischen Kenngrößen wie sphärische Wirkung, astigmatische Wirkung und prismatische Wirkungsdifferenz wurde der Wellenfrontfehler (fünf verschiedene Blickrichtungen) als Kenngröße verwendet, um die optische Qualität bestimmen zu können und damit die Schutzbrillengeometrie zu optimieren.

Ergebnisse: Alle vermessenen Oberflächen waren sphärisch (maximale Abweichung 'peak-to-valley' zur best-fit Sphäre: 0,132 mm). Bis auf die sphärische Wirkung der Schutzbrille Axcont ($-0,07 \text{ m}^{-1}$) lagen bereits vor der Optimierung alle optischen Kenngrößen innerhalb der besten optischen Toleranz, die in den Normen vorgegeben wird. Nach der Optimierung konnte der Wellenfrontfehler um 1% auf 0,150 λ (Windor/Infield), um 63% auf 0,194 λ (Axcont/Bolle) und um 55% auf 0,199 λ (2720/3 M) gesenkt werden, ohne die gemessene Dicke zu unterschreiten.

* Corresponding author: Benedikt Zelzer, Experimental Ophthalmology, Saarland University, Kirrberger Straße 100, D-66421 Homburg/Saar, Germany.
Tel.: +49 6841/16-22327; Fax: +49 6841/16-21241.
E-mail: benedikt.zelzer@uks.eu (B. Zelzer).

Keywords: Protective eyewear, safety spectacles, ray tracing, oblique viewing, wavefront error

Schlussfolgerung: Durch eine geschickte Optimierung kann die theoretische Abbildungsqualität von reellen Schutzbrillendesigns zum Teil verbessert werden. Ein gutes optisches Design wirkt Einflüssen durch Prozessparameter schwankungen in der Produktion entgegen.

Schlüsselwörter: Augenschutz, Schutzbrillen, Raytracing, Blickfeld, Wellenfrontfehler

Introduction

Many working conditions, such as in mechanical workshops or in laboratories with chemical substances, require adequate eyewear protecting against mechanical and chemical hazards. Personal protective eyewear, such as safety spectacles, face shields and goggles, are highly effective and help to avoid most ocular injuries if used properly [1,2]. To ensure a minimum standard for safety spectacles, the ISO, DIN EN and ANSI standards focus on the protective effect – e.g. the resistance against flying objects or splashing chemicals [3–6]. Optical requirements for safety spectacles are restricted to a non-refractive effect, stray light properties of the material and transparency. In spectacle optics gaze angles play an important role which induce additional aberrations, the so-called oblique astigmatism. This oblique astigmatism itself originates from various optical aberrations such as primary and higher order astigmatism and coma. Therefore, every spectacle lens represents a more or less good compromise – apart from the main visual point through the lens (the paraxial space) for which it has been optimized [7]. Inferior image quality may lead to headache, less acceptance of the safety device and may therefore cause eye injuries [8]. According to Lombardi et al., 30% of the interviewed persons complained about potential somatic effects, such as headaches, dizziness or nausea [9]. In the last few years the development of eye protection concentrated on increasing the acceptance by introducing softer earpieces for the frame, working with more flexible materials and the design of modern frames. In refractive spectacle glass design it is common to calculate centered lenses using conventional algorithms and then decenter and tilt these lenses for using them as safety spectacle. This altered position in front of the eye results in a change (increase) of oblique astigmatism or prism. Improving this simple method, future spectacle designs implemented spherocylindrical and prismatic shapes to reduce these aberrations. Analytical modeling of these decentered and tilted surfaces requires sophisticated algorithms [7,10]. With modern raytracing software it is possible to analyze and optimize even complex optical systems numerically.

The refractive power requirements of safety spectacles are standardized in DIN EN 166/167, ANSI Z87 and ISO 4849, as well as other national standards [3–6]. The thresholds for the best defined optical classification (optical class 1) are:

$\pm 0.06 \text{ m}^{-1}$ for spherical power, 0.06 m^{-1} for astigmatic power and $-1/-0.75$ to 0.25 cm/m for horizontal prism imbalance. Are safety spectacles, manufactured with the label “optical class 1 product”, as good as defined by those standards?

The purpose of this study was to develop simulation models created on the basis of real safety spectacles available on the market for the enhancement of existing safety spectacles and for generating new lens designs. We measured and analyzed three existing spectacles with a ‘modern curved design’ and similar radius of curvature and used the measured surface data to create the theoretical spectacle model. Starting with a recalculated backside radius we optimized the backside surface of this model as a function of the refractive error.

Material and Methods

Simulation model

The spectacle model used for simulation is shown in Figure 1. All four surfaces are spherical, defined by radius of curvature, center of curvature and offset.

Optimization of safety spectacles was done in three steps. In step one measured parameters are used to create the spectacle model and to simulate the optical performance. Considering measurement inaccuracies (quantified in Table 1) this optical performance represents the finished product after molding process and assembly. In step two the backside radius of curvature R_2 is recalculated ($R_{2,\text{calc}}$) and necessarily the distance $R_{12,Z}$ is adapted to retain the correct thickness. In the last step the parameters R_2 , $R_{2,\text{off}}$ and $R_{12,Z}$ – defining the backside surface – are iteratively optimized, with $R_{2,\text{calc}}$ as starting value for R_2 . The other parameters R_1 and $R_{1,\text{off}}$ – defining the front surface – are restricted by several predefined constraints like design or application and were fixed. This optimized parameter set is used to simulate the optical performance again.

Measurement setup

Surface data of three safety spectacles (Fig. 2) was acquired using a commercially available phase measuring deflectometer (PMD) (SpecGAGE, 3D-Shape GmbH, Erlangen, Germany) [11]. The system was equipped with two cameras

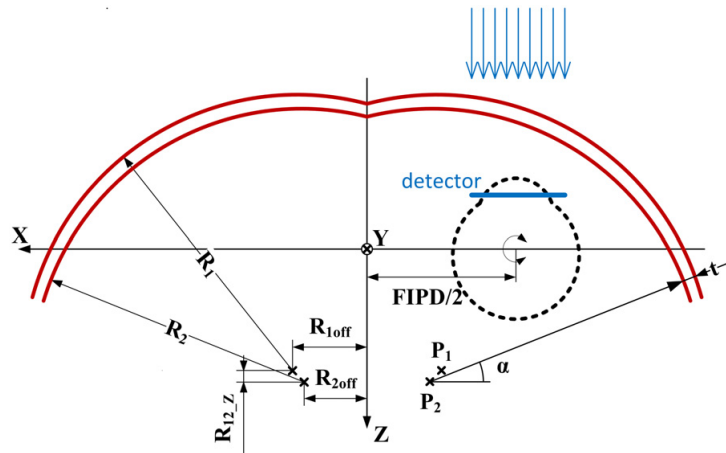


Figure 1. Cross section of the symmetric safety spectacle model (thick solid lines) used for simulation. The geometry definition is illustrated on the left side. The thickness could be calculated with the parameter at the lower right side (input: P_1 , P_2 , α). The dotted line illustrates the location of the eye at the far interpupillary distance (FIPD). The detector (thick solid line) is placed at the level of the iris. A plane wavefront (ray bundle, 10 mm diameter) propagates through the optical surfaces and is recorded by the detector - optical aberrations are considered at the pupillary plane. The simulation of oblique viewing is emulating physiological eye movements due to defining an appropriate rotation center [22].

Table 1

Complete data and numerical results of the compared geometries. All information required for modeling the geometry is listed in the first section. After thickness information the third section shows the simulation results defined by the standards and the last section lists the wavefront errors in wavelength (pupil diameter 10 mm). The wavefront errors combine all aberrations (excluding tilt and piston). The weighted wavefront errors combine each direction as shown in Figure 3. Due to symmetry the vertical prism imbalance is zero for all geometries.

Manufacturer/model	state	Infield/Windor		Bolle/Axcont		3M/2720		
		measured	optimized	measured	optimized	measured	optimized	accuracy
R₁		64.99	64.99	50.16	50.16	54.98	54.98	0.15
global deviation from fitted sphere (PV)		0.034		0.037		0.044		
R₂		64.16	64.12	48.98	49.16	53.83	53.99	0.15
global deviation from fitted sphere (PV)	(mm)	0.054		0.132		0.050		
R_{1off}		10.62	10.62	21.05	21.05	17.60	17.60	0.01
R_{2off}		10.62	10.66	21.05	21.07	17.55	17.56	0.01
R_{12,Z}		1.44	1.44	1.28	1.70	1.32	1.67	
thickness (measured, $\alpha=90^\circ$)		2.26		2.46		2.48		0.02
thickness (measured, $\alpha=30^\circ$)	(mm)	1.57		1.77		1.77		0.02
thickness (calculated, $\alpha=90^\circ$)		2.27	2.31	2.46	2.70	2.47	2.66	
thickness (calculated, $\alpha=30^\circ$)		1.54	1.54	1.81	1.81	1.84	1.84	
spherical power	(1/m)	0.009	0.008	-0.070	0.008	-0.055	0.001	
astigmatic power	(1/m)	0.009	0.011	0.003	0.009	0.007	-0.010	
horizontal prism imbalance	(cm/m)	-0.059	0.005	-0.228	-0.039	-0.339	-0.180	
straight view (rms)		0.051	0.049	0.380	0.037	0.300	0.014	
20° temporal (rms)		0.074	0.065	0.354	0.056	0.240	0.062	
20° upwards (rms)	(λ)	0.164	0.172	0.566	0.250	0.483	0.250	
20° nasal (rms)	(632.8nm)	0.349	0.339	0.809	0.456	0.780	0.511	
20° downwards (rms)		0.164	0.172	0.566	0.250	0.483	0.250	
weighted (rms)		0.150	0.149	0.521	0.194	0.443	0.199	



Figure 2. Measured three safety spectacles - Axcont/Bolle (top left), Windor/Infield (top right) and 2720/3 M (bottom).

enabling measurement of absolute position in space (absolute stereo-deflectometry).

This PMD is specified with a maximum field of view of $80 \times 80 \text{ mm}^2$, an absolute accuracy of $\pm 3 \mu\text{m}$ peak-to-valley (PV) and a curvature measurement error of 0.01 m^{-1} [12]. After defining each spectacle surface as spherical (to be proved later on), five parameters have to be set: front radius of curvature (R_1), backside radius of curvature (R_2), offset of the front sphere center of curvature to the symmetry axis ($R_{1\text{off}}$), offset of the backside sphere center of curvature ($R_{2\text{off}}$) and the distance of front and backside center of curvature along the z axis ($R_{12,Z}$) (Fig. 1).

Analysis of the front and the backside surface data was performed using GOM Inspect (Gesellschaft für Optische Messtechnik mbH, Braunschweig, Germany). Radius of curvature identification (R_1, R_2) was done by fitting a sphere (best-fit) to the front and backside surface of each safety spectacle [13]. The deviation between the fitted sphere and the measured surface is quantified by the global deviation (PV) listed in Table 1. The offset parameter ($2 \cdot R_{1\text{off}}$ and $2 \cdot R_{2\text{off}}$) were determined by calculating the Euclidean distance in 3D-space between both fitted front spheres and both fitted backside spheres. The last missing parameter ($R_{12,Z}$) was approximated ($R_{12,Z} = R_2 + t - R_1$) using the measured center thickness (t) at $\alpha = 90^\circ$. The center thickness measurement points were defined by the line of sight while wearing the safety spectacles and looking straight ahead and the calculated Euclidean distance ($2 \cdot R_{2\text{off}}$). Center thickness was measured with a caliper (1044SB, Mitutoyo Deutschland GmbH, Neuss, Germany).

Backside radius of curvature recalculation

The first step for (re-)calculating the backside radius of curvature (simplification: geometric optical thick lens) is the

Gullstrand equation [14]:

$$F = F_1 + F_2 - \frac{t}{n} \cdot F_1 \cdot F_2 \quad (1)$$

The refractive power (F) should yield zero (ideal; no impairment of vision), the outer medium is air and F_1, F_2 and t can be written as:

$$F_1 = \frac{n-1}{R_1}; F_2 = \frac{1-n}{R_2}; t = R_{12,Z} \quad (2)$$

Inserting Eq. (2) in Eq. (1) results in the calculated $R_{2,\text{calc}}$ as a function of the radius of curvature R_1 , the refractive index n and the thickness t :

$$R_{2,\text{calc}} = \frac{R_1 \cdot n - t \cdot n + t}{n} \quad (3)$$

Additionally the distance ($R_{12,Z}$) is adapted to keep the right thickness:

$$R_{12,Z} = R_2 + t - R_1 \quad (4)$$

The calculated $R_{2,\text{calc}}$ and the adapted $R_{12,Z}$ is used as a starting parameter for the optimization step.

Simulation setup

The simulation environment was established using the ray-tracing software ASAP (version 2010 V1R1 SP 2, Breault Research Organisation, Tucson, USA). All components (spectacle model, sources and the eyes) were centered vertically ($Y=0$) on a level with the line of vision looking straight ahead (Fig. 1). Furthermore the horizontal distance of the eyes was set to 64 mm – the standardized far interpupillary distance (FIPD) [15]. The detector was placed at the level of the iris at $Z=-11.2 \text{ mm}$, 3.8 mm behind the anterior corneal surface [16,17]. The vertex distance between the cornea and the backside of all three safety spectacles was measured with a standard spectacle on a standard head from the side in ten subjects with a digital caliper (Absolute 500-776, Mitutoyo Deutschland GmbH, Neuss, Germany) as $12.5 \pm 1.5 \text{ mm}$, which is close to the generic value of 12 mm used in ophthalmic optics. In addition, the distance between the anterior corneal surface and the rotation center of the eye was set to 15 mm as measured by Fry and Hill [18]. Standard material, used for producing safety spectacles, is polycarbonate with a refractive index within the range of $n(\lambda = 380 \text{ nm}) = 1.62$ and $n(\lambda = 780 \text{ nm}) = 1.57$ [19,20]. The material for simulation was defined as uncoated polycarbonate (Makrolon®, Bayer, $n(\lambda = 632.8 \text{ nm}) = 1.581$). Simulations were performed monochromatically at a wavelength at 632.8 nm (HeNe laser) for further comparison to a wavefront measurement system [21]. Due to symmetry only one side of the symmetric spectacle was used for simulation.

Optical tests and simulated directions of gaze

Each spectacle model was tested for spherical and astigmatic power, prism imbalance and wavefront error. According to DIN EN 167 we used a collimated 30×1 ray bundle (20 mm diameter) propagating through front and backside surface to determine the refractive power. The minimal and maximal refractive power was determined by rotating the ray bundle around the optical axis about 180 degrees. The mean value of minimal and maximal refractive power defined the spherical power and the difference defines the astigmatic power. In addition we simulated two small diverging ray bundles (0.2 mm diameter, 0.9°) propagating through a perfect lens (focal length 1000 mm, perfect imaging of an object plane at infinity and no spherical aberration of the principal points) hitting the detector plane in one spot. Including the spectacle model, positioned in front of the perfect lens, both ray bundles hit the detector at different locations. The prism imbalance is defined as the vertical and the horizontal distance between both points in centimeters divided by two (distance between spectacles and detector is 2 m). Additionally, the wavefront error was derived. The basic concept was tracing of a plane wavefront (Fig. 1) by tracing a ray bundle (100 × 100 rays, aperture: 10 mm diameter) through the front and backside surface of the spectacle to the detector plane. The complete array of rays yields an optical path difference map (OPD map), showing the wavefront error including all aberrations. The root mean square (RMS) of the complete OPD map excluding tilt and piston errors was used as parameter for optimization.

Simulation of vision through different areas of the shield was performed by holding the spectacle fix while rotating detector plane and the light source around the defined center of rotation (Fig. 1). Four areas of off-axis vision were defined to evaluate the field of view. As shown in Figure 3 the spectacle was tested with off-axis inclinations of 20° in each direction in addition to the straight view. This was chosen according to the largest amount of eye movement before turning the head [22].

Taking the higher importance of the straight view into account, the RMS values were weighted for each direction as follows: straight view – factor 3, view upwards – factor 2, temporal view – factor 2, view downwards – factor 2 and nasal view – factor 2. This weighted RMS parameter, which describes the optical performance of each spectacle model, was used as optimization parameter.

The safety spectacles were optimized for an infinite object, using the far interpupillary pupil distance FIPD. To fulfill the safety standard requirements, personal protective eyewear had to provide a minimal lens thickness. The measured thicknesses of all safety spectacles defined the minimal thicknesses of the relating models. Thickness measurement and thickness calculation was performed at two angles alpha ($t_1, \alpha_1=90^\circ$ and $t_2, \alpha_2=30^\circ$) as defined in Figure 1.

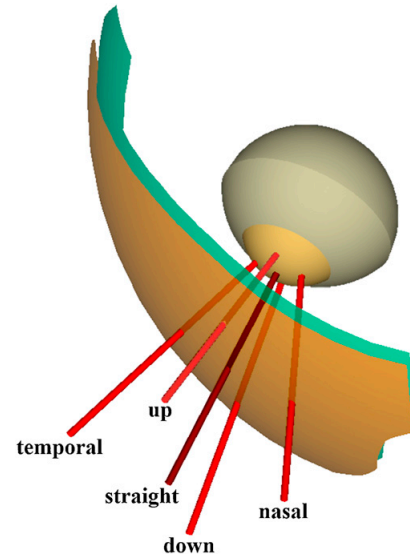


Figure 3. Three dimensional sketch of one half of the safety spectacle model generated in ASAP. The lines represent different inclinations of beams traced through the two optical surfaces onto the detector (here illustrated as eye). Each beam is tilted by 20° relative to the straight view (darker line).

Parameter range

The parameter range for optimization was $R_{2,\text{calc}} \pm 2$ mm, $R_{2,\text{off}} \pm 0.1$ mm and $R_{12,Z} + 0.5$ mm/–0.2 mm. With a step width of 0.01 mm for each parameter, all combinations (401·21·71 = 597891) were simulated for each safety spectacle. To speed up raytrace time the simulation of each parameter combination was canceled when a) the center thickness $t_1 < t_{1,\text{measured}}$ or $t_1 > 3$ mm; b) the temporal thickness $t_2 < t_{2,\text{measured}}$ or $t_2 > 3$ mm; c) the prism imbalance was higher than simulated with measured parameters; d) the wavefront error of the straight view was higher than simulated with measured parameters. Only parameter sets which remained within these limits were recorded. The parameter set which resulted in the best optical performance (smallest weighted wavefront error) was used as optimized model geometry.

This three-step-procedure (simulation of measured geometry, recalculating the backside radius of curvature and simulation of the optimized backside surface) was repeated for all three spherical safety spectacles.

Results

Three different safety spectacles Windor (tinted, optical class 1) (Infield, Solingen, Germany), Axcont (clear, optical class 1) (Bolle, Suresnes, France) and 2720 (clear, optical

class 1) (3 M, St. Paul, USA) were measured, recalculated and optimized (Table 1). For better comparison all three types of safety spectacles had similar radii of curvature between 49 and 65 mm. The parameter set and simulation results are given for both steps. Due to assumed perfect symmetry the vertical prism imbalance was zero for all geometries and is not further mentioned.

The calculated backside radius of curvature of each safety spectacle is: $R_{2,calc,Windor} = 64.16$ mm, $R_{2,calc,Axcont} = 49.26$ mm, $R_{2,calc,2720} = 54.07$ mm. We additionally adapted the parameter $R_{12,Z}$: $R_{12,Z,Windor} = 1.44$ mm, $R_{12,Z,Axcont} = 1.56$ mm, $R_{12,Z,2720} = 1.56$ mm before starting the optimization.

The results of each safety spectacle before and after optimization are shown in Figures 4–6. The limits of safety spectacles (optical class 1) without refractive power defined by DIN EN 167 are: spherical power $\pm 0.06 \text{ m}^{-1}$, astigmatic power 0.06 m^{-1} and horizontal prism imbalance -0.75 cm/m (base out) to 0.25 cm/m (base in) and marked as dashed lines.

After backside surface optimization each model showed a higher center thickness and the same temporal thickness. The center thickness increased by 2% (Windor), 10% (Axcont) and 8% (2720).

The weighted wavefront error of Windor/Infield was reduced by 1% to 0.150λ . The weighted wavefront error of Axcont/Bolle was reduced by 63% to 0.194λ . And the weighted wavefront error of 2720/3 M was reduced by 55% to 0.199λ . Spherical and astigmatic power of each optimized spectacle is between -0.01 and 0.01 m^{-1} – a sixth of the limit for optical class 1.

Discussion

The limits of spherical power, astigmatic power and prism imbalance for the best optical class 1 are considerably strict, but only given for the straight view [3–6]. In spectacle optics oblique angles of gaze with large angles up to 20° play an important role when eyes converge to focus close objects. Additionally there are a couple of parameters affecting the optical performance of safety spectacles, i.e. optical design, tool polishing, manufacturing process and deformed glasses due to simple frame design. Joining a basic safety spectacle model, industrial recommendations and five different viewing directions with the raytracer ASAP, we optimized three measured safety spectacles. This could be also repeated with an arbitrary front surface resulting in a new spectacle design. We defined all surfaces to be spherical, because of maximal global deviations (PV) between the measured surface and the fitted sphere of 0.132 mm. Optimization was done by recalculating the backside radius of curvature, which was used as starting value for iteratively changing the model parameter, an additional cancelling strategy when exceeding the defined limits and finding the minimal wavefront error of different viewing directions.

Due to the higher scratch sensitivity of polycarbonate, a scratch resistant coating is often used [23]. However, the coating was not included in the simulation due to a lack of information about the different coating properties of all measured safety spectacles.

We simulated the spherical power, astigmatic power and prism imbalance. Nearly all measured and simulated spectacles were better than the limits defined by the standards. Only the safety spectacle Axcont results in little higher spherical power (-0.07 m^{-1}) as permitted in optical class 1 (limit -0.06 m^{-1}). However the simulated spherical power does not necessarily agree with the real spectacle as we did not measure the refractive index of the spectacle. The best performance with only minor potential for improvements showed the Windor/Infield.

Having almost the same anterior radius of curvature (between 49 and 65 mm), the same labeled protection class F (resistance test, 45 m/s, 0.86 g steel bullet [4]) and the same optical class, the measured central and temporal thickness of Windor is about 0.2 mm less than both others.

The only changes between the measured and the optimized Windor model were an altered backside radius of curvature ($R_{2,diff} < 1\%$, negligible) and an altered $R_{2,off}$ ($R_{2,off,diff} = -0.04$ mm), affecting mostly the prism imbalance (reduction of 92%). All other simulated values were nearly the same. This effect of small differences in both center of curvature offsets ($R_{1,off}$, $R_{2,off}$) is used for compensating the prism imbalance.

The difference between the measured and the optimized spectacle sums up all optical degradations through the manufacturing process, if the optimized parameter sets should have been used by the manufacturer as optical designs. This denotes a good manufacturer process in the case of the spectacle Windor.

Each simulated model (both measured and optimized) had its maximum wavefront error when converging for the close-up range. If the eyes were rotated nasally (Fig. 1) oblique viewing through both surfaces was more present. This led to higher aberrations, due to oblique astigmatism.

Becken et al. optimized spectacle lenses for sport applications in a similar way using the matrix formalism which is known for calculation of toric intraocular lenses [7]. Their analytical optimization approach uses theoretically defined spherocylindrical surface shapes, while our numerical simulation could be used with arbitrary, free form surface shapes as well. The sportive spectacle lenses described by Becken were designed to provide a large covering area (wind protection and large gaze angles) and therefore have to be decentred and tilted. The surfaces were iteratively changed until the refractive data met the predefined criteria. The goal was to individually optimize refractive spectacle lenses for each wearer. In contrast to this, safety spectacles cannot be individualized, have to be non refractive spectacles and while reducing aberrations it is very important to keep the protection effect.

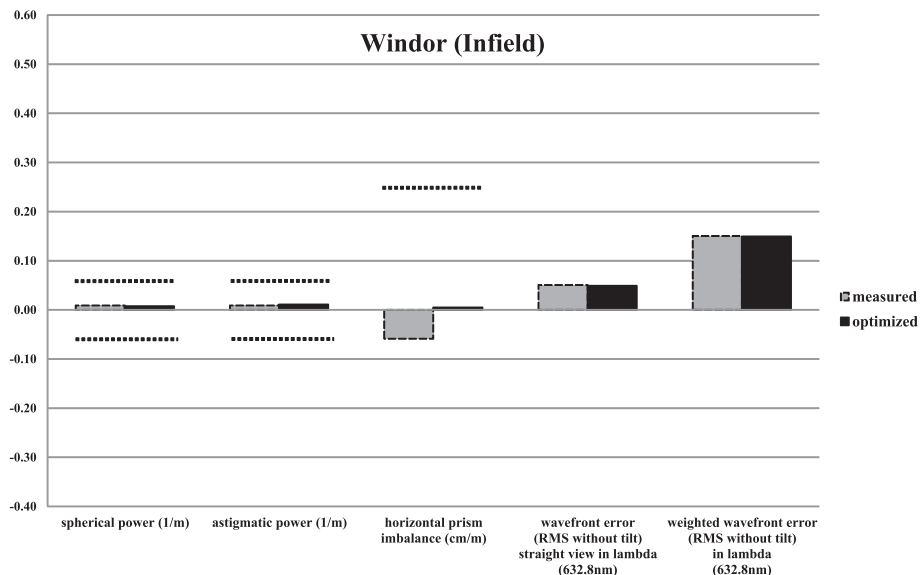


Figure 4. Optical performance of the safety spectacle Windor (Infield) with measured parameter set and optimized parameter set. The first three values in the diagram are related to the test setups defined in DIN EN 166/167. Limits defined by standards are shown as dashed line. As mentioned in Figure 3 the weighted wavefront error combines each direction.

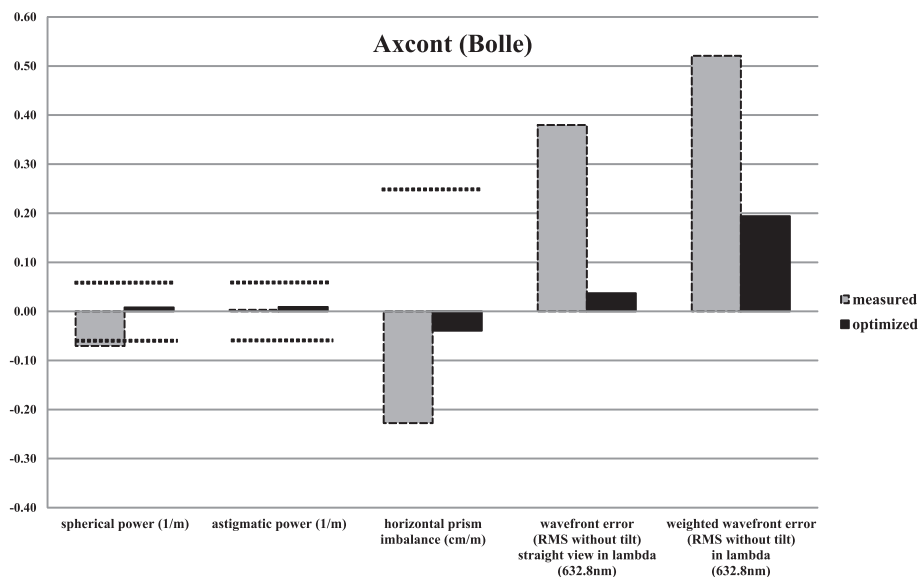


Figure 5. Optical performance of the safety spectacle Axcont (Bolle) with measured parameter set and optimized parameter set. The first three values in the diagram are related to the test setups defined in DIN EN 166/167. Limits defined by standards are shown as dashed line. As mentioned in Figure 3 the weighted wavefront error combines each direction.

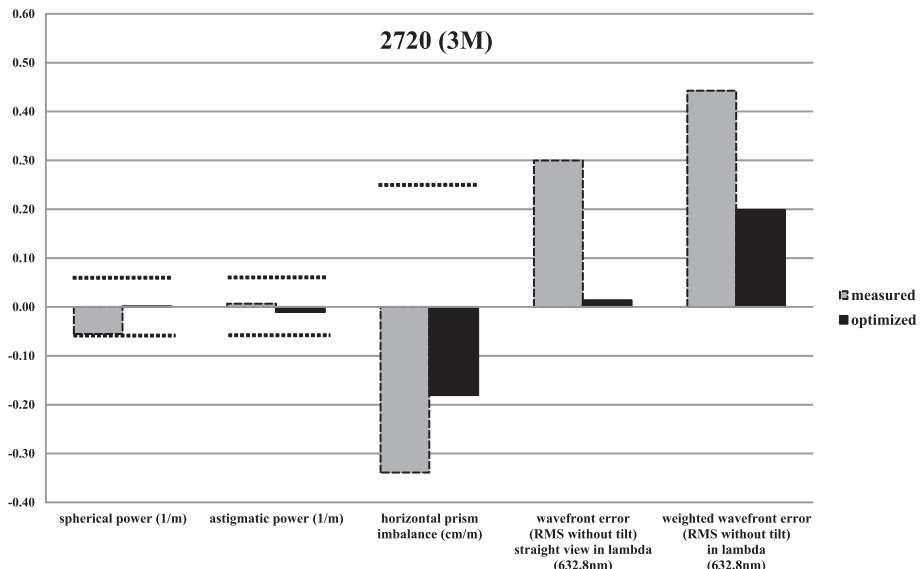


Figure 6. Optical performance of the safety spectacle 2720 (3 M) with measured parameter set and optimized parameter set. The first three values in the diagram are related to the test setups defined in DIN EN 166/167. Limits defined by standards are shown as dashed line. As mentioned in Figure 3 the weighted wavefront error combines each direction.

Our study had some limitations. The optimization was based on one specific parameter set of a standardized human head model, i.e. constant interpupillary distance. Dogson et al. defined the mean FIPD range as 50 - 75 mm [15]. It is understood, that a single curved shield cannot be appropriate for this wide range. The optimization could be repeated for FIPD values other than 64 mm as well. Real individualization is not possible as safety spectacles are supposed to be a low cost but high quality product. Individuals with extreme FIPDs are candidates for different safety spectacle geometries (e.g. plane ones). The simulation was performed monochromatically to speed up raytrace time. Results could be improved by using a polychromatic white light model in order to account for chromatic aberration as well. Our results are only valid for distance vision, where the incident wavefront is a plane. When wearing protective eyewear, a lot of work has to be done in the near distance range. Near distance simulation requires divergent wavefronts and modifications in weighting of the visual field due to binocular convergence. However, the region of interest for optimization would be a different one when converging to a close point. These additions are subject of future investigations. A comparison of simulated aberrations to measured aberrations with a Shack-Hartmann sensor is planned [21].

In conclusion, we have created a software platform to optimize safety spectacles or generating new designs, without dropping below a minimum thickness needed for protecting the eye. Three different safety spectacles, currently available on the market, were compared to show the wavefront error

reduction and directions of optimization. Limits are given, due to the wide range of far interpupillary distances and the optimization for distance vision. A good optical design counteracts degradation by parameter variation throughout manufacturing processes.

Conflict of interest

The authors have no proprietary interest in the development or marketing of this or any competing instrument or piece of equipment.

Acknowledgements

The authors gratefully acknowledge financial support by the Bavarian Research Foundation (Grant number: AZ-874-09), Munich, Germany. Part of the methods have been presented on the Dreiländertagung Medizinische Physik 2011 in Vienna.

References

- [1] Speck A, Zelzer B, Eppig T, Langenbucher A. Experimental assessment of eye protection efficiency against high speed projectiles. *Z Med Phys* 2012, <http://dx.doi.org/10.1016/j.zemedi.2012.06.008>.
- [2] Mancini G, Baldasseroni A, Laffi G, Curti S, Mattioli S, Violante FS. Prevention of work related eye injuries: long term assessment of the effectiveness of a multicomponent intervention among metal workers. *Occup Environ Med* 2005;62:830–5.

- [3] International Standards. Personal eye-protectors - Specifications. ISO 4849 1981.
- [4] Deutsches Institut für Normung e.V. Personal eye protection - specifications. DIN EN 166 2001.
- [5] Deutsches Institut für Normung e.V. Personal eye protection – optical test methods. DIN EN 167 2001.
- [6] American National Standard. Occupational and educational personal eye and face protection devices - spectacles. ANSI Z87.1 2003.
- [7] Becken W, Seidemann A, Altheimer H, Esser G, Uttenweiler D. Spectacle lenses in sports: optimization of the imaging properties based on physiological aspects. *Z Med Phys* 2007;17:56–66.
- [8] Fong LP, Taouk Y. The role of eye protection in work-related eye injuries. *Aust N Z J Ophthalmol* 1995;23:101–6.
- [9] Lombardi D, Verma S, Brennan M, Perry M. Factors influencing worker use of personal protective eyewear. *Accid Anal Prev* 2009;41:755–62.
- [10] Blendowske R. Oblique Central Refraction in Tilted Spherocylindrical Lenses. *Optom Vis Sci* 2002;79:68–73.
- [11] 3D-Shape GmbH. SpecGAGE 3D (2011). http://www.3d-shape.com/produkte/pmid_d.php. accessed: 21.10.2011.
- [12] Knauer M, Veit K. Vermessung spiegelnder Oberflächen - eine Aufgabe der optischen 3D-Sensorik. *Photonik* 2004;4:62–4.
- [13] Speck A, Zelzer B, Langenbucher A, Eppig T. Deflectometry for surface inspection and shape fidelity analysis for manufacturing and polishing of safety spectacle molds. *DGfO Proceedings* 2012; 113:P30.
- [14] Diepes H, Blendowske R. Das dicke Brillenglas. In: Optik und Technik der Brille. Heidelberg: Optische Fachveröffentlichung GmbH; 2002. p. 8.
- [15] Dogson NA. Variation and extrema of human interpupillary distance. *Proc SPIE* 2004;5291:36–46.
- [16] Atchison AD, Smith G. The human eye: an overview. In: Optics of the Human Eye. 1st Edition Edinburgh: Elsevier; 2000. p. 9.
- [17] Thibos L, Applegate R, Schwiegerling J, Webb R. Standards for Reporting the Optical Aberrations of Eyes. *J Refract Surg* 2002;18:652–60.
- [18] Fry GA, Hill WW. The center of rotation of the eye. *Am J Optom Arch Am Acad Optom* 1962;39:581–95.
- [19] Dain S. Materials for occupational eye protectors. *Clin Exp Optom* 2012;95:129–39.
- [20] Bayer Makrolon (2001). <http://plastics.bayer.com/plastics/emea/de/produkt/apc/datenblaetter/docId-2386/A8043.pdf>. accessed: 22.11.2011.
- [21] Eppig T, Zoric K, Speck A, Zelzer B, Götzemann J, Nagengast D, et al. Wave-front analysis of personal eye protection. *Opt Express* 2012;20: 17806–15.
- [22] Schober H. Das Blickfeld und Umblickfeld. In: Das Sehen. Leipzig: VEB; 1970. p. 96.
- [23] Rychwalski P, Packwood E, Cruz O, Holds J. Impact resistance of common spectacle and safety lenses to airgun and rimfire projectiles. *J AAPOS* 2003;7:268–73.

Available online at www.sciencedirect.com

SciVerse ScienceDirect

6 Literaturverzeichnis

- [1] American National Standards Institute (2003) Occupational and educational personal eye and face protection devices. ANSI Z 87.2 – 2003
- [2] Berufsgenossenschaft der Feinmechanik und Elektrotechnik (2001) BGR 192 - Benutzung von Augen- und Gesichtsschutz. Bericht, Berufsgenossenschaftliche Zentrale für Sicherheit und Gesundheit
- [3] Bull N (2007) Mandatory use of eye protection prevents eye injuries in the metal industry. Occup Med (Lond) 57(8):605–606
- [4] Bundesministerium für Arbeit und Soziales (2009) Versorgungsmedizin - Verordnung mit den Versorgungsmedizinischen Grundsätzen. Bericht K710, Bundesministerium für Arbeit und Soziales. URL <http://www.bmas.de/SharedDocs/Downloads/DE/PDF-Publikationen/k710-versorgungsmed-verordnung.html>. Zugriff am 25.05.2013
- [5] Chou BR, Gupta A, Hovis JK (2005) The effect of multiple antireflective coatings and center thickness on resistance of polycarbonate spectacle lenses to penetration by pointed missiles. Optom Vis Sci 82(11):964–969
- [6] Deutsches Institut für Normung e.V. (2002) Persönlicher Augenschutz – Anforderungen. DIN EN 166: 2001
- [7] Deutsches Institut für Normung e.V. (2002) Persönlicher Augenschutz – Nicht-optische Prüfverfahren. DIN EN 168: 2001
- [8] Deutsches Institut für Normung e.V. (2002) Persönlicher Augenschutz – Optische Prüfverfahren. DIN EN 167: 1995
- [9] Dietrich TM, Kleinschmidt R, Meyer HJ (1992) Veränderte Ursachen und Folgen schwerer Augenverletzungen - Ein Vergleich von 197 eigenen stationär behandelten Patienten mit anderen Literaturberichten. Klin Monatsbl Augenheilkd 201(10):216–220

- [10] Eppig T, Zoric K, Speck A, Zelzer B, Götzelmann J, Nagengast D, Langenbucher A (2012) Wave-front analysis of personal eye protection. *Opt Express* 20(16):17806–17815
- [11] Fong L, Taouk Y (1995) The role of eye protection in work-related eye injuries. *Aust Nz J Ophthalmol* 23(2):101–106
- [12] Forrest KYZ, Cali JM, Cavill WJ (2008) Use of protective eyewear in U.S. adults: results from the 2002 national health interview survey. *Ophthalmic Epidemiol* 15(1):37–41
- [13] van Griethuysen JPS, Glardon R, Karapatis NP (1997) Injection molds behavior and lifetime characterization - Concept and design of a standard measurement method. In: Solid Freeform Fabrication Proceedings. 317–324
- [14] Hannes-Hinrich Heissmeyer and Hellmut Neubauer (1965) Experimentelle Untersuchungen zur durchdringenden Meiselsplitterverletzung des Auges. *Graefes Arch Clin Exp Ophthalmol* 168:599–613
- [15] Hartewig K (2009) Der verhüllte Blick: Kleine Kulturgeschichte der Sonnenbrille. Jonas-Verlag. URL <http://books.google.de/books?id=tKBaPgAACAAJ>. Zugriff am 25.05.2013
- [16] Hauptverband der gewerblichen Berufsgenossenschaften (2004) BGV-A1 - Grundsätze der Prävention. Bericht, Hauptverband der gewerblichen Berufsgenossenschaften
- [17] Hod Y, Geyer O (2005) Eye injuries caused by rotating wire brushes. *Harefuah* 144(4):239–40
- [18] Hoffmann B, Rostek R (2002) Arbeitsunfallstatistik. Bericht, Hauptverband der gewerblichen Berufsgenossenschaften
- [19] International Organization for Standardization (1981) International standard 4849. ISO 4849: 1981
- [20] International Organization for Standardization (1981) International standard 4854. ISO 4854: 1981
- [21] Knauer M, Kaminski J, Häusler G (2004) Phase measuring deflectometry: a new approach to measure specular free-form surfaces. *P Soc Photo-Opt Ins* 5457:366–376
- [22] Knauer M, Richter C, Hybl O, Kaminski J, Faber C, Häusler G (2009) Deflektometrie macht der Interferometrie Konkurrenz. *tm – Technisches Messen*

76(4):175–181

- [23] Knauer M, Veit K (2004) Vermessung spiegelnder Oberflächen – eine Aufgabe der optischen 3D-Sensorik. *Photonik* 4(4):62–64
- [24] Langenbucher A, Eppig T, Nagengast D, Börret R (2010). IVOS - Improved Vision for Occupational Eye Safety. Projektantrag
- [25] Lombardi D, Verma S, Brennan M, Perry M (2009) Factors influencing worker use of personal protective eyewear. *Accident Anal Prev* 41(4):755–762
- [26] Mackiewicz J, Machowicz-Matejko E, Salaga-Pylak M, Piecyk-Sidor M, Zagórski Z (2005) Work-related, penetrating eye injuries in rural environments. *Ann Agric Environ Med* 12(1):27–29
- [27] Oliver AL, Chou BR (1993) A ballistic evaluation of the impact resistance of spectacle lens materials. *Optom Vis Sci* 70(10):822–827
- [28] Rychwalski P, Packwood E, Cruz O, Holds J (2003) Impact resistance of common spectacle and safety lenses to airgun and rimfire projectiles. *J AAPOS* 7(7):268–273
- [29] Speck A, Zelzer B, Langenbucher A, Eppig T (2012) Deflectometric analysis of high volume injection molds for production of occupational eye wear. Im Revisionsprozess bei *Z Med Phys*
- [30] Speck A, Zelzer B, Langenbucher A, Eppig T (2012) Deflectometry for surface inspection and shape fidelity analysis for manufacturing and polishing of safety spectacle molds. *DGAO Proc* 113:p30
- [31] Speck A, Zelzer B, Langenbucher A, Eppig T (2013) Quality control of injection molded eyewear using non-contact deflectometry. Im Revisionsprozess bei *Appl Opt*
- [32] Zelzer B, Speck A, Langenbucher A, Eppig T (2013) Theoretical model for design and analysis of protectional eyewear. *Z Med Phys* 23(2):120–128

7 Publikationsverzeichnis

Eigene wissenschaftliche Originalarbeiten

- [1] Zelzer B, Speck A, Langenbucher A, Eppig T (2013) Theoretical model for design and analysis of protectional eyewear. *Z Med Phys* 23(2):120–128.
- [2] Speck A, Zelzer B, Eppig T, Langenbucher A (2013) Experimental assessment of eye protection efficiency against high speed projectiles. *Z Med Phys* 23(1):71–76.
- [3] Eppig T, Zoric K, Speck A, Zelzer B, Götzemann J, Nagengast D, Langenbucher A (2012) Wave-front analysis of personal eye protection. *Opt Express* 20(16):17806–17815.
- [4] Speck A, Zelzer B, Speich M, Börret R, Langenbucher A, Eppig T (2012) Deflectometric analysis of high volume injection molds for production of occupational eye wear. *Z Med Phys*; im Revisionsprozess.
- [5] Speck A, Zelzer B, Kannengießer M, Langenbucher A, Eppig T (2013) Inspection of freeform intraocular lens topography by phase measuring deflectometric methods. *Appl Opt* 52(18):4279–4286.
- [6] Speck A, Zelzer B, Langenbucher A, Eppig T (2012) Deflectometry for surface inspection and shape fidelity analysis for manufacturing and polishing of safety spectacle molds. *DGaO Proc* 113:p30.
- [7] Langenbucher A, Szentmáry N, Speck A, Seitz B, Eppig T (2013) Calculation of power and field of view of keratoprostheses. *Ophthal Physiol Opt* 33(4):412–419.
- [8] Eppig T, Speck A, Gillner M, Nagengast D, Langenbucher A (2012) Photochromic dynamics of ophthalmic lenses. *Appl Opt* 51(2):133–138.

- [9] Janunts E, Speck A, Hasenfus A, Seitz B, Langenbucher A (2012) Computerized approach for laser-assisted penetrating keratoplasty using MEL70 excimer laser system. *Biomed Res Int; im Revisionsprozess.*
- [10] Speck A, Zelzer B, Langenbucher A, Eppig T. Quality control of injection molded eyewear using non-contact deflectometry. *Appl Opt; im Revisionsprozess.*

Kurzveröffentlichungen, Vorträge und Poster mit zitierfähigem Abstrakt

- [1] Speck A. Augenschutz gegen äußere Einwirkung – Normative Anforderungen und richtige Auswahl der passenden Sicherheitsbrille. Refraktive Herbstakademie, Linz, Österreich, 2012.
- [2] Speck A, Zelzer B, Eppig T. Wellenfronten & Wellenfrontmessung. Refraktive Herbstakademie, Linz, Österreich, 2011.
- [3] Speck A. Optimierung von Arbeitsschutzbrillen mit optischer Premiumqualität – Messplatz zur Erfassung der Oberflächengeometrie. Aktuelle Stunde, Homburg, Deutschland, 2011.
- [4] Eppig T, Gillner M, Speck A, Langenbucher A. Charakterisierung photochromer Brillengläser. Arbeitskreis Ophthalmische Optik, Aalen, Deutschland, 2011.
- [5] Speck A, Zelzer B, Langenbucher A, Eppig T. Deflectometry for surface inspection and shape fidelity analysis for manufacturing and polishing of safety spectacle molds. Poster P30, 113. Jahrestagung der DGaO, Eindhoven, Niederlande, 2012.
- [6] Speck A. Untersuchung verschiedener SCADA-Systeme auf Eignung zur Prozesssteuerung, Visualisierung und Datenarchivierung an Extrusionsanlagen. Postervorstellung an der Georg-Simon-Ohm-Hochschule, Nürnberg, Deutschland, 2010.
- [7] Zelzer B, Speck A, Langenbucher A, Eppig T. Schutzbrillen mit optischer Premiumqualität. Poster P05.08, 3 Ländertagung der ÖGMP, DGMP und SGSSMP, Wien, Österreich, 2011.
- [8] Zelzer B, Speck A. Optimierung von Arbeitsschutzbrillen mit optischer Premiumqualität: Softwareplattform zur Simulation von Abbildungsfehlern. Arbeitskreis Ophthalmische Optik, Aalen, Deutschland, 2011.

8 Danksagung

An dieser Stelle bedanke ich mich bei meiner Familie und meinen Freunden für die Unterstützung während meiner Doktorarbeit. Danken möchte ich Prof. Dr. Alfred Leitl, Dr. Annette Walter und Dr. Stefan Arnold für den Weg zur Medizintechnik und schließlich zum Promotionsvorhaben.

Insbesondere möchte ich meinem Doktorvater Prof. Dr. Achim Langenbucher danken, der mir die Promotion überhaupt ermöglicht hat und mir mit etlichen Fachgesprächen und seiner Kompetenz im medizinischen und technischen Sinn den richtigen Weg wies. Ganz besonderer Dank gebührt meinem Betreuer Dr. Timo Eppig für die schier unzähligen Diskussionen, Ansätze und seine Geduld im Hinblick auf meine Arbeit in der Experimentellen Ophthalmologie. Die hervorragende Betreuung hat maßgeblich zum Erfolg meiner Arbeit im Institut beigetragen.

Benedikt Zelzer danke ich für das angenehme Zusammenleben, beruflich als Kollege und die konstruktive Zusammenarbeit als Projektpartner, wie auch privat als Mitbewohner im Saarland. An die gemeinsame Zeit in der Wohngemeinschaft werde ich mich gerne erinnern.

Meinen Kollegen Marc Kannengießer, Melanie Gillner, und Dr. Edgar Janunts möchte ich für die interessanten Gespräche und Auseinandersetzungen in der Optik und Physik und ganz besonders für die private Unterstützung danken.

Herzlich danke ich dem gesamten Institut für Experimentelle Ophthalmologie für die sehr schöne Zeit.

Alexis Speck
Juni 2013

